Deep-Sea Research II 58 (2011) 358–377

Contents lists available at ScienceDirect

Deep-Sea Research II

journal homepage: www.elsevier.com/locate/dsr2

Spatially-resolved taxon-specific phytoplankton production and grazing dynamics in relation to iron distributions in the Equatorial Pacific between 110 and 140°W

Karen E. Selph [1,*], Michael R. Landry [2], Andrew G. Taylor [2], Eun-Jin Yang [3], Christopher I. Measures [1], Jingjing Yang [4], Michael R. Stukel [2], Stephanie Christensen [1], Robert R. Bidigare [5]

[1] Department of Oceanography, University of Hawaii at Manoa, Honolulu, HI 96822, USA
[2] Scripps Institution of Oceanography, University of California at San Diego, La Jolla, CA 92093-0227, USA
[3] Division of Polar Climate Research, Korea Polar Research Institute, KORDI, Songdo Techno Park, Songdo, Yeonsu, Incheon 406-840, South Korea
[4] Department of Earth Sciences, University of Oxford, Parks Road, Oxford OX1 3PR, United Kingdom
[5] Hawaii Institute of Marine Biology, University of Hawaii at Manoa, Honolulu, HI 96822, USA

ARTICLE INFO

Available online 25 August 2010

Keywords:
Equatorial Pacific
110 - 140°W
4°N to 4°S
Phytoplankton growth
Grazing
Iron

ABSTRACT

Phytoplankton dynamics were investigated in the eastern equatorial Pacific at 32 stations sampled during two cruises (December 2004 and September 2005). Based on standing stock analyses from HPLC pigments, flow cytometry and microscopy, we used a modified 2-treatment approach of the seawater dilution method to estimate taxon-specific phytoplankton growth and mortality rates in 8-depth per station profiles. These data were complemented by contemporaneous measurements of dissolved iron (Fe). The stations encompassed an equatorial zonal gradient (110 to 140°W) of diminishing eastward Fe availability in the euphotic zone from upwelling of the Equatorial Undercurrent (EUC). Latitudinal variation was assessed by meridional transects at 110 and 140°W. Overall, euphotic zone averaged growth rates were $0.53 \pm 0.17\ d^{-1}$ (total chlorophyll *a*), $0.34 \pm 0.15\ d^{-1}$ (divinyl chlorophyll *a*) and $0.86 \pm 0.32\ d^{-1}$ (fucoxanthin). Microzooplankton grazing accounted for 50-60% of daily production of eukaryotic algae, whereas essentially all growth of phototrophic prokaryotes was consumed daily. Fucoxanthin, representing diatoms, was a minor component of the accessory pigments, but diatom growth rates were both significantly higher than other taxonomically defined groups and dropped off more sharply with depth (low light level). Strikingly, no spatial or temporal trends were seen in the 256 growth rate measurements for each measured pigment. However, the diminishing eastward equatorial Fe gradient was associated with deepening subsurface pigment maxima and decreasing surface-layer pigment stocks (down to the 8% light level). In addition, integrated standing stocks of total chlorophyll *a* and *Prochlorococcus* (divinyl chlorophyll *a*) were strongly correlated with integrated iron at equatorial upwelling stations, yet no correlation with Fe was seen for any of the eukaryotic groups, including diatoms. This latter result is contrary to expectations from previous Fe addition experiments (*in situ* or in bottles), where diatom biomass increased relative to other phytoplankton. We hypothesize that the natural supply of Fe to the base of the euphotic zone from the EUC is less favorable for diatoms because of light limitation. Rather, new Fe is rapidly incorporated into a small phytoplankton-dominated community in the deep euphotic zone, and tightly coupled grazing control results in a system regulated by return of recycled Fe.

1. Introduction

The regulation of phytoplankton population dynamics in the eastern equatorial Pacific (EEP) is of great interest to understanding our changing world because this area represents the largest oceanic efflux of carbon dioxide to the atmosphere on the planet (Murray et al., 1994; Feely et al., 2002; Takahashi et al., 2002). Upwelling at the equator in the EEP brings macronutrient-rich waters to the surface ($>4\ \mu M$ surface nitrate), yet chlorophyll standing stocks there are relatively low (0.2-0.3 $\mu g\ liter^{-1}$), leading to its designation as a HNLC area (Minas et al., 1986; Levitus et al., 1993; Barber et al., 1996a, b; Chavez et al., 1991). The EEP has been modeled as a chemostat (Frost and Franzen, 1992), which receives regular inputs of nutrients from the base of the euphotic zone and exports water from the surface to the north and south through divergence. Past research has shown that, like

* Corresponding author.
E-mail address: selph@hawaii.edu (K.E. Selph).

0967-0645/$ - see front matter © 2010 Elsevier Ltd. All rights reserved.
doi:10.1016/j.dsr2.2010.08.014

other HNLC areas, the limiting nutrient in this system is iron (Kolber et al., 1994; Martin et al., 1994; Coale et al., 1996a, b; Coale et al., 1998). Microzooplankton grazing is also a key component of phytoplankton regulation in this system, as shown through modeling and experimental studies (Frost and Franzen, 1992; Landry et al., 1997).

Previous research in the EEP focused on phytoplankton growth and microzooplankton grazing rates in the mixed layer or deep chlorophyll maximum, and usually reported data from only a few stations or experiments per study (Landry et al., 1995a, b, 2003; Verity et al., 1996; Latasa et al., 1997). While these data have allowed us to understand how this system operates in a general sense, they leave us with an incomplete view of euphotic zone processes. To more fully understand this system, the traditional multi-bottle design of the dilution experiment was reduced to a 2-treatment approach to generate a rate profile of 8 depths at each station. This resulted in the data set reported here, which is comprised of 256 experiments, conducted over two cruises and a wide geographical area (equatorial stations from 110° to 140°W, as well as meridional transects at 110° and 140°W).

When a community is incubated in a bottle for 24 hours, it is perhaps inevitable that changes occur in that community relative to in situ populations. For instance, if the light levels experienced by the bottle-held community are somewhat higher or lower than in situ levels, then the phytoplankton populations have time to adjust their photosynthetic apparatus accordingly. This is a well-recognized problem with pigment-based incubation data (Landry et al., 1995a, 2003; Latasa et al., 1997). Previous studies did not have the data to realistically adjust growth rates for all such imbalances, particularly for the eukaryotic taxa. Thus, another novelty of the present approach was the combined use of microscopical, flow cytometric and HPLC pigment analyses to estimate pigment:biomass at the beginnings and ends of the incubations, so that changes in cellular pigment contents over the course of our incubations could be quantified and used appropriately to resolve rate estimates.

Another issue that has complicated the interpretation of past research in the equatorial Pacific is the lack of Fe data to directly compare to the biological parameters measured. While Fe has been measured in this area, it was usually not determined at the same places or times as biological rate parameters. This is a problem, as it appears that there are year-to-year differences in the amount of Fe supplied to the euphotic zone through upwelling, depending upon how much Fe is entrained in the EUC to the west and the depth of the EUC (Gordon et al., 1997; Kaupp et al., 2011). Also, Fe varies significantly in the EUC at different longitudes, notably being stripped out of the EUC in its eastward transport across the Pacific. This project had the advantage of contemporaneous measurements of iron and rates, so that meaningful comparisons could be made.

Considering the large zonal and meridional spatial area covered in our sampling, the detailed depth profiles for phytoplankton growth and mortality at each station and the Fe data gathered, this data set allows us to look for the first time in substantial detail at the vertical and horizontal spatial scales of variability in process rates for co-occurring dominant phytoplankton groups.

2. Materials and methods

2.1. Water-column sampling

This research was conducted aboard the R/V *Roger Revelle* in December 2004 and September 2005 over a spatially extensive area of the eastern equatorial Pacific as shown in Fig. 1. On the 2004

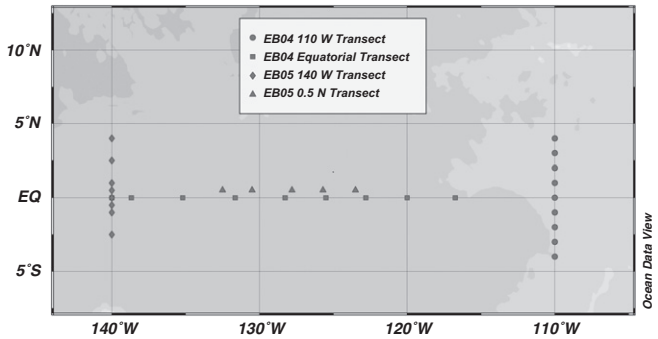

Fig. 1. Map of the study area. Stations were occupied in the Equatorial Pacific between 110 and 140°W and 4°N to 4°S, on board two cruises, one in September 2004 and one in December 2005 on board the R/V *Roger Revelle*.

cruise (hereafter referred to as "EB04"), samples were collected on a zonal transect of 9 stations along the equator from 140°W to 117°W with 1 - 3° longitudinal spacing, as well as an equatorial station at 110°W. The EB04 cruise also included a meridional transect at 110°W consisting of 9 stations spaced at 1° intervals from 4°N to 4°S, and two additional stations at 0.5°N and 0.5°S close to the equator. During the 2005 cruise (hereafter "EB05"), a zonal transect of 6 stations was sampled at 0.5°N, the first station at 140°W, and the rest approximately 2° of longitude apart from 132.5° to 123.5°W. In addition, sampling and experimental studies were conducted on a meridional transect of 8 stations at 140°W from 4°N to 2.5°S.

Acoustic Doppler Current Profiler (ADCP) data were obtained from a ship-mounted RDI, 150 kHz ADCP system. These data were processed into 8 db bins, and a final data set consisting of 1 db estimates of the U (eastward) and V (northward) components of velocity were produced courtesy of J. Hummon (University of Hawaii at Manoa, http:soest.hawaii.edu/sadcp). Current velocities are not available from this instrumentation at depths shallower than ~20 m.

At each station, depth profiles of basic hydrographic data (temperature, salinity, macronutrients) were taken with a CTD-rosette system, using acid-cleaned 10-L PVC Niskin bottles with Teflon-coated springs. The CTD profile was done consistently in the early morning (typically 0300-0400) well before sunrise, and samples were taken for flow cytometric analyses of microbial community abundance, for HPLC pigment-based biomass and for experimental studies of growth and mortality rates. For each profile, we sampled 8 depths in the euphotic zone corresponding to light levels of 0.1, 0.8, 5, 8, 13, 31, 52 and 100% of incident solar irradiance (I_o). These light levels were chosen to correspond to the calibrated light levels of our deck incubators.

A trace metal clean rosette system, consisting of 12 GOFLO bottles mounted on a powder-coated frame, was used to collect samples for estimates of dissolved (<0.2-μm filtrate) Fe at each sampling station. This system is described in Measures et al. (2008), and further details of sample collection and analyses are provided in Kaupp et al. (2011). Briefly, dissolved Fe was determined using the spectrophotometric Flow Injection Analysis method of Measures et al. (1995), with a detection limit for Fe of 0.079 nM and a precision of 2.63%. Nitrate+nitrite was determined at sea on a Bran and Luebee Autoanalyzer II (Dugdale et al., 2007).

Contour plots of the data were generated using Ocean Data View (Schlitzer, 2006). A "VG gridding" algorithm was used for variable resolution in a rectangular grid where grid spacing varies accordingly to data density.

2.2. HPLC pigment analyses

Phytoplankton pigments were analyzed using high-performance liquid chromatography (HPLC) according to the methods of

Bidigare et al. (2005). Sample volumes of 1.2 - 2.3 L were concentrated onto 25-mm GF/F filters (Whatman). The filters were wrapped in foil, then flash-frozen in liquid nitrogen and stored at -80 °C until analysis. Pigments were extracted in 3 ml of 100% acetone in the dark at 0 °C for 24 h. Canthaxanthin (50 μl in acetone) was added as an internal standard in all samples. Prior to analysis, the pigment extracts were vortexed and centrifuged to remove cellular debris.

Subsamples were injected into a Varian 9012 HPLC system equipped with a Varian 9300 autosampler, a Timberline column heater (26 °C), and a Spherisorb 5-μm ODS2 analytical column (4.6 × 250 mm) and corresponding guard cartridge. Eluting peaks were monitored with an UV/vis absorption detector (436 and 450 nm). Pigment peaks were identified by comparison of retention times with those of pure standards and extracts prepared from algal cultures of known pigment composition.

The major pigments presented are total chlorophyll a (TChl*a*), mono-vinyl chlorophyll a (MVChl*a*), divinyl chlorophyll a (DVChl*a*), the photoprotective carotenoid pigment zeaxanthin (ZEAX), as well as dominant accessory pigments (i.e., those present at concentrations $\geq$ 4 ng liter^{-1}) 19′-hexanoyloxyfucoxanthin (HEX), 19-butanoyloxyfucoxanthin (BUT), fucoxanthin (FUCO), and peridinin (PER). Taxonomic assignments for each major pigment are based on known pigment compositions (Wright and Jeffrey, 1987; Buma et al., 1991; Vaulot et al., 1994; Jeffrey and Vesk, 1997). TCHL*a* is comprised of MVChl*a* and DVChl*a*. MVChl*a* is found in all eukaryotic phytoplankton, as well as *Synechococcus*, a prokaryote. DVChl*a* is found only in *Prochlorococcus*. HEX and BUT are found in both prymnesiophytes and pelagophytes, but HEX is found in higher concentrations in prymnesiophytes (Arpin et al., 1976; Gieskes and Kraay, 1986; Wright and Jeffrey, 1987), whereas BUT is the dominant accessory pigment of pelagophytes (Vesk and Jeffrey, 1987; Wright and Jeffrey, 1987, Bjørnland and Liaaen-Jensen, 1989; Andersen et al., 1993). These two groups may also contain some FUCO, but here we assume that FUCO is indicative of diatoms. PER is found only in dinoflagellates, although it is absent in some taxa (e.g., Millie et al., 1993), so these data are likely minimum estimates of the contribution of this group. Violaxanthin (chrysophytes), alloxanthin (cryptophytes), prasinoxanthin (prasinophytes), and lutein (chlorophytes) were either not detected or only occasionally detected ($<$4 ng liter^{-1}) and so these groups are not considered important components of the equatorial phytoplankton community. ZEAX is found in *Synechoccocus* and *Prochlorococccus*, prasinophytes and chlorophytes. Since diagnostic pigments for the two eukaryotic groups are very low in this system, ZEAX reflects mainly the pigment content of the phototrophic bacteria, *Synechococcus* and *Prochlorococcus*.

2.3. Flow cytometric analyses

Picoplankton abundances were estimated using flow cytometry (FCM). FCM samples (2 ml) were preserved (0.5% paraformaldehyde, v/v, final concentration), frozen in liquid nitrogen, then transferred for storage in a −80 °C freezer until analysis. Thawed samples were stained with Hoechst 33342 (1 μg ml^{-1}, v/v, final concentration) at room temperature in the dark for 1 h (Monger and Landry, 1993; Campbell and Vaulot, 1993). Aliquots (100 μl) were analyzed for populations of phytoplankton and heterotrophic bacteria using a Beckman-Coulter EPICS Altra flow cytometer mated to a Harvard Apparatus syringe pump for volumetric sample delivery. Simultaneous (co-linear) excitation of the plankton was provided by two water-cooled 5 W argon ion lasers, tuned to 488 nm (1 W) and the UV range (200 mW). The optical filter configuration distinguished populations on the basis of chlorophyll *a* (red fluorescence, 680 nm), phycoerythrin (orange fluorescence, 575 nm), DNA (blue fluorescence, 450 nm), and forward and 90° side scatter signatures. Calibration beads (0.5 and 1.0-μm yellow-green beads and 0.5-μm UV beads) were used as fluorescence standards. Raw data (listmode files) were processed using the software FlowJo (Treestar Inc., www.flowjo.com).

Prochlorococcus and *Synechococcus* abundances from FCM analyses were converted to biomass estimates using mixed-layer estimates of 32 and 101 fg C cell^{-1}, respectively (Garrison et al., 2000; Brown et al., 2008). These values are also quite comparable to those (35 and 100 fg C cell^{-1}) that were used in a synthesis of microbial community structure in the equatorial Pacific (Landry and Kirchman, 2002).

2.4. Microscopical analyses

Biomass estimates for eukaryotic phytoplankton were determined by digitally-enhanced epifluorescence microscopy as described by Taylor et al. (2011). Cells $<$10-μm in size were enumerated from 50-ml aliquots preserved with paraformaldehyde (0.5% final concentration), stained with proflavin (0.33% w/v) and DAPI (10 μg ml^{-1}) and mounted onto black 0.8-μm black Nuclepore filters. Larger cells (microplankton) were enumerated on 500-ml subsamples, preserved according to Sherr and Sherr (1993), stained with proflavin and DAPI, and mounted onto 8-μm black Nuclepore filters.

The slides were imaged and digitized at 630 × (nanoplankton) or 200 × (microplankton) with a Zeiss AxioVert 200M inverted epifluorescence microscope with a Zeiss AxioCam HR color CCD digital camera. Cell biovolumes (BV; μm^3) were determined from length (L) and width (W) measurements using the formula for a prolate sphere (BV=0.524 L W H), where cell height (H) on the filters was empirically determined to be 0.5 W for naked flagellates (including dinoflagellates). Carbon (C; pg cell^{-1}) biomass was computed from BV from the equations of Menden-Deuer and Lessard (2000): $C=0.216 \times BV^{0.939}$ for non-diatoms, and $C=0.288 \times BV^{0.811}$ for diatoms.

2.5. Phytoplankton growth and grazing rates

We used the seawater dilution method (Landry and Hassett, 1982) to determine growth and mortality rates of the phytoplankton; however, the approach was modified from a regression-based, multi-treatment experiment at a given depth, to a design that allowed 2-point daily rate estimates from multiple depths (Landry et al., 1984, 2011). Daily experiments were set up using water collected from each of the 8 light depths sampled by the pre-dawn CTD sampling (Section 2.1). For each depth, one 2.8-L polycarbonate bottle was filled with whole seawater while a second bottle received a measured 1.8 L volume of filtered seawater (0.1-μm Suporcap filter capsule pre-washed with 10% trace-metal grade HCl followed by Milli-Q and seawater rinses) from the same depth before being topped up gently with whole seawater (total volume ~2.8 L), resulting in a ~36% dilution treatment. Paired experimental bottles were placed in surface seawater-cooled, shipboard incubators, each screened with neutral density plastic film (Cotech) to the relative light level ($\%I_o$) at the depth of sample collection, and incubated for 24 h. The water-filled incubators were calibrated to incident PAR on site using a Biospherical QSL-100 Quantum Scalar Irradiance Meter. Initial and final (24-h) samples were taken for fluorometric chlorophyll *a*, phytoplankton accessory pigments (HPLC), picoplankton abundance (FCM), as well as nano- and micro-plankton abundance and biomass (microscopy).

Taxon-specific instantaneous rates of phytoplankton growth (μ, d^{-1}), net growth (k, d^{-1}) and mortality due to microzooplankton grazing (m, d^{-1}) were estimated from initial and final experiment results according to Landry et al. (2008). Briefly, growth (μ) and mortality (m) rates were calculated from the undiluted (whole seawater) and diluted bottles' net growth rates (k and k′, respectively) as follows:

$$k = \mu - m \quad (1)$$

$$k' = \mu - (D \times m) \quad (2)$$

where D=fraction of whole seawater in diluted treatment. Solving these two equations for μ and m, leads to:

$$m = (k' - k)/(1 - D) \quad (3)$$

$$\mu = k + m \quad (4)$$

Growth rates based on measured changes in pigment concentrations were corrected for photoadaptation effects and unbalanced growth of cell pigment content by accounting for changes in the ratios of pigment (HPLC) to biomass (microscopy or FCM) between initial and final samples. For diatoms, for example, we used initial and final ratios of FUCO to microscopically estimated diatom biomass to compute net pigment rate of change during the incubation. Similarly, the microscopical biomass estimates for all autotrophs were used to normalize the rates from TChl*a*, while eukaryotic autotroph+*Synechococcus* biomass estimates were used for normalizing MVChl*a*, and HEX (prymnesiophytes) and BUT (pelagophytes) were normalized by the biomass of 2-10 μm eukaryotic autotrophs. Biomass of eukaryotic autotrophs between 10-20 μm was used to normalize PER, since dinoflagellates dominated this size class. In the case of *Prochlorococcus*, we used final:initial changes in the natural log-ratio of red fluorescence per cell, as measured by the flow cytometer, to correct growth rates based on the pigment DVChl*a*. However, microscopy-based estimates of final carbon biomass were not available for every depth and every experiment on both cruises because of data processing difficulties, so all the available data (number of data points per light level: 20 ± 7.5 (average ± one standard deviation of the mean), minimum=9, maximum=32) were averaged over both cruises for each light level, then applied to the individual rate data of each station. Without applying these corrections, the estimated growth rates were higher. For instance, the euphotic-zone averaged growth rates based on TChl*a* would have been 40% higher, while diatom rates based on FUCO would have been nearly double those reported.

To estimate total euphotic zone growth and mortality rates at each station, pigment-based rates were weighted by the amount of phytoplankton carbon biomass at each light level and then averaged over the euphotic zone. The weighted carbon:pigment factor for each taxonomic group at each light level (WCP_i) was calculated by dividing the initial estimate of the population-specific carbon biomass from microscopy by the initial taxon-specific pigment concentration and averaging all these estimates by light level. The resulting estimate of carbon biomass was used to determine the proportion of the water column occupied by the relevant population, and this was used to weight the rates for depth averaging. The calculations for this are as follows:

$$B_i = WCP_i \times P_i \times D_i \quad (5)$$

$$F_i = \frac{B_i}{\sum B_i} \quad (6)$$

$$r_i = r_D \times D_i \quad (7)$$

$$r_{avg} = \sum (F_i \times r_i) \quad (8)$$

where B_i=carbon biomass over depth interval i (μg C m^{-2}), WCP_i=weighted carbon:pigment at light level i, P_i=pigment concentration at light level i (μg m^{-3}), D_i=depth interval (m), F_i=fraction of total carbon over depth interval i, r_i=rate (μ or m) over depth interval i, r_D=rate at depth i, and r_{avg}=average rate over the euphotic zone. Production and net production (production−consumption) rates for components of the phytoplankton community (units of μg pigment m^{-2} d^{-1}) were determined by multiplying the relevant biomass-adjusted depth-weighted rate by the log-mean depth-integrated concentration of the relevant pigment.

2.6. Statistical tests

The statistical tests used to compare pigment standing stocks and rate data between transects and between each other were Kruskal-Wallis single factor analysis of variance by ranks, followed by the Tukey test for non-parametric multiple comparisons, modified as appropriate for unequal sample sizes and/or tied ranks (Zar, 1984). The t-test was used when only two groups were compared.

3. Results

3.1. Currents and hydrography

Figs. 2 and 3 show ADCP-derived current velocities (cm sec^{-1}) and density (sigma-t, kg m^{-3}), as well as iron (Fe, nM) and nitrate+nitrite (N+N, μM) data, for the upper 120 m of the water column, arranged by cruise (EB04 and EB05) and by zonal (equator and 0.5°N) and meridional (140°W and 110°W) transects. All transects reveal the dominant subsurface easterly flow of the EUC (Equatorial Undercurrent) centered on the equator (Fig. 2). The equatorial transect (EB04) shows that the shallowest depth of 100 cm sec^{-1} velocities shoaled from ~110 m at 140°W to ~90 m at 110°W (Fig. 2A). The 0.5°N transect in the following year (EB05) also sliced through the EUC from 140°W to ~128°W, as indicated by the 100 cm sec^{-1} eastward velocities, but the 121°W station, with eastward currents of ≤60 cm sec^{-1} at 80-120 m, did not intersect the EUC on that cruise (Fig. 2B). In contrast, the water at shallower depths (20 to ~60 m at the equator; 20-30 m at 0.5°N) generally flowed westward at speeds up to 20 cm sec^{-1}, but westward velocity was higher (up to 50 cm sec^{-1}) from ~118 to 125°W at the equator (Fig. 2A & B). These variations in east-west velocities comprise the U component of the equatorial currents.

Elevated meridional flows, the V component of current velocity, signaled the presence of tropical instability waves in our study area. Flanking the surface westward flowing region on the equator, meridional flows extending to 120 m were to the north from ~114-118°W (20-40 cm sec^{-1}) and to the south at ~122-126°W (20-40 cm sec^{-1}) (Fig. 2A). Strong flows to the north and south were also seen at 0.5°N, centered at ~129°W and 126°W, respectively (Fig. 2B). Strong southerly flow encompassed the entire euphotic zone at 140°W, 0.5°N, diminishing with depth.

Eastward flow of the EUC was the prominent feature of the transects at 140°W (EB05) and 110°W (EB04), showing a core velocity of ~110 cm sec^{-1} at the base of the euphotic zone in both locations (U component, Fig. 2C, D). EUC velocities decreased with latitude, flanking the equator and reaching 0 cm sec^{-1} at ~2°S and 2°N. North and south of the EUC (2-4°N and 2-4°S), current flows were to the west. At 140°W, there was an area of rapid (50 cm sec^{-1}) southward flow centered (50-60 m) at 0.75°N

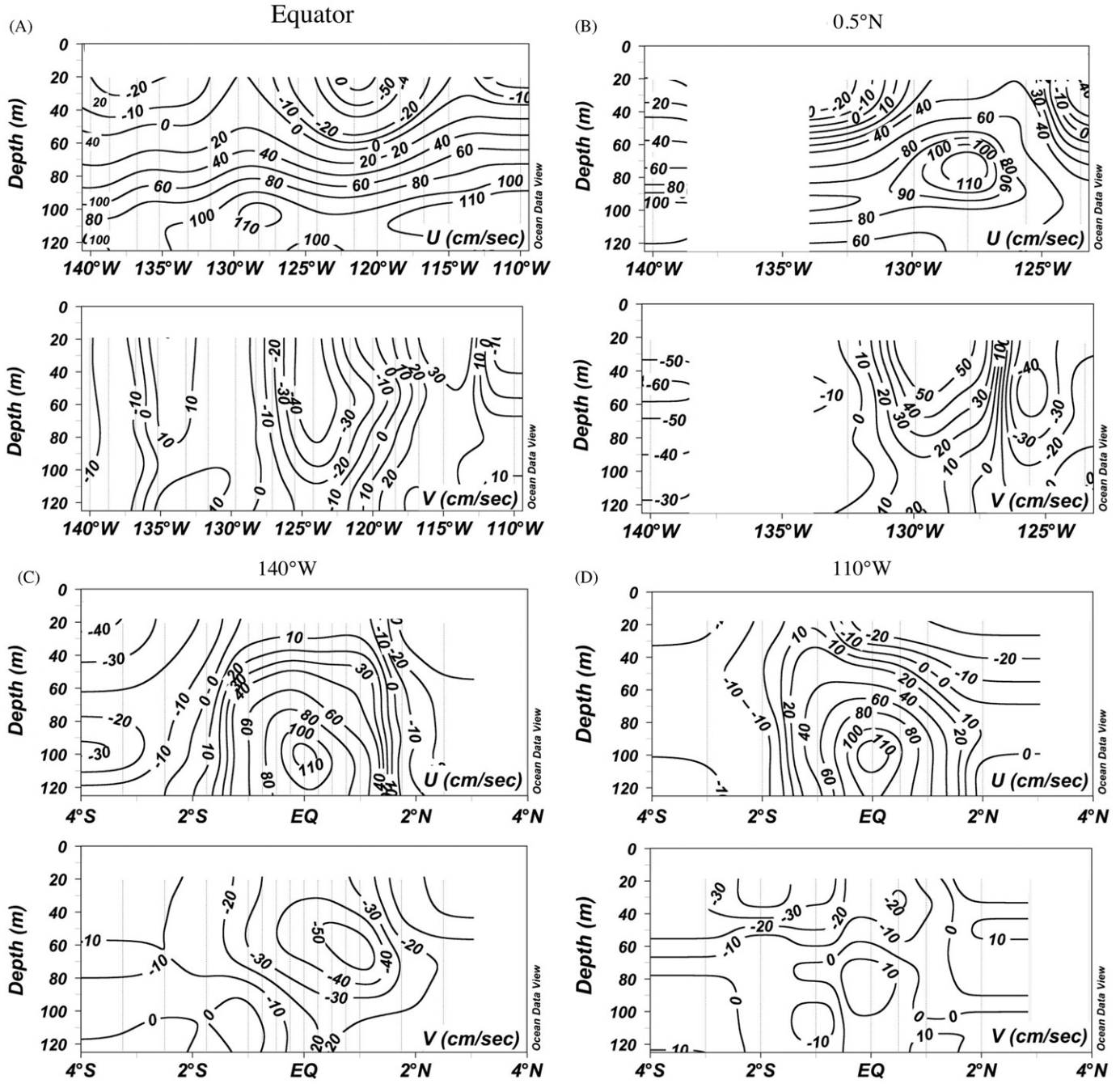

Fig. 2. ADCP Current Data arranged by transect. The current data (cm sec^{-1}) are separated into U (E-W) and V (N-S) components, with positive values for U to the east and for V to the north. Blank areas of the figures denote an absence of data for that area.

(V component, Fig. 2C). At 110°W, the only significant meridional flows (40 cm sec^{-1}) were at the surface at ~2°S (V component, Fig. 2D).

3.2. Dissolved macronutrients

Concentrations of Nitrate+Nitrite (N+N) exceeded 2 μM in surface waters of all transects (Fig. 3, left panels). Zonal sections along the equator and 0.5°N showed surface concentrations of 5-7 μM N+N, except at 0.5°N, 132.5°W and 120°W where surface concentrations dropped to 2-4 μM (Fig. 3A, B). N+N concentrations > 10 μM were seen in the EUC (70 to ~120 m), except at 2.5°N, 140°W where N+N was ~7 μM at 100 m. On the equatorial transect, the nitracline depth shoaled to the east, from about 100 m at 140°W to ~60 m at 110°W. The nitracline was relatively constant (~60 m) from 140°W to 120°W on the 0.5°N zonal transect, but deepened to ~80 m at 121°W, the easternmost point of that transect (Fig. 3B).

Along the meridional transect at 140°W, the nitracline depth was ~60-70 m in the equatorial region (1°S-2°N), and shallowest at 1°S where doming isopycnals from upwelling were evident (Fig. 3C). Nitraclines deepened to ~110 m polewards of the equatorial region. Along the 110°W transect, the nitracline was ~70 m south of the equator (to 4°S), shoaled to ~20 m at the equator, and deepened to 50 m by 4°N (Fig. 3D). Patterns in phosphate and silicate concentrations were similar to those of N+N (data not shown). Phosphate ranged from 0.05 to 2.65 μM in

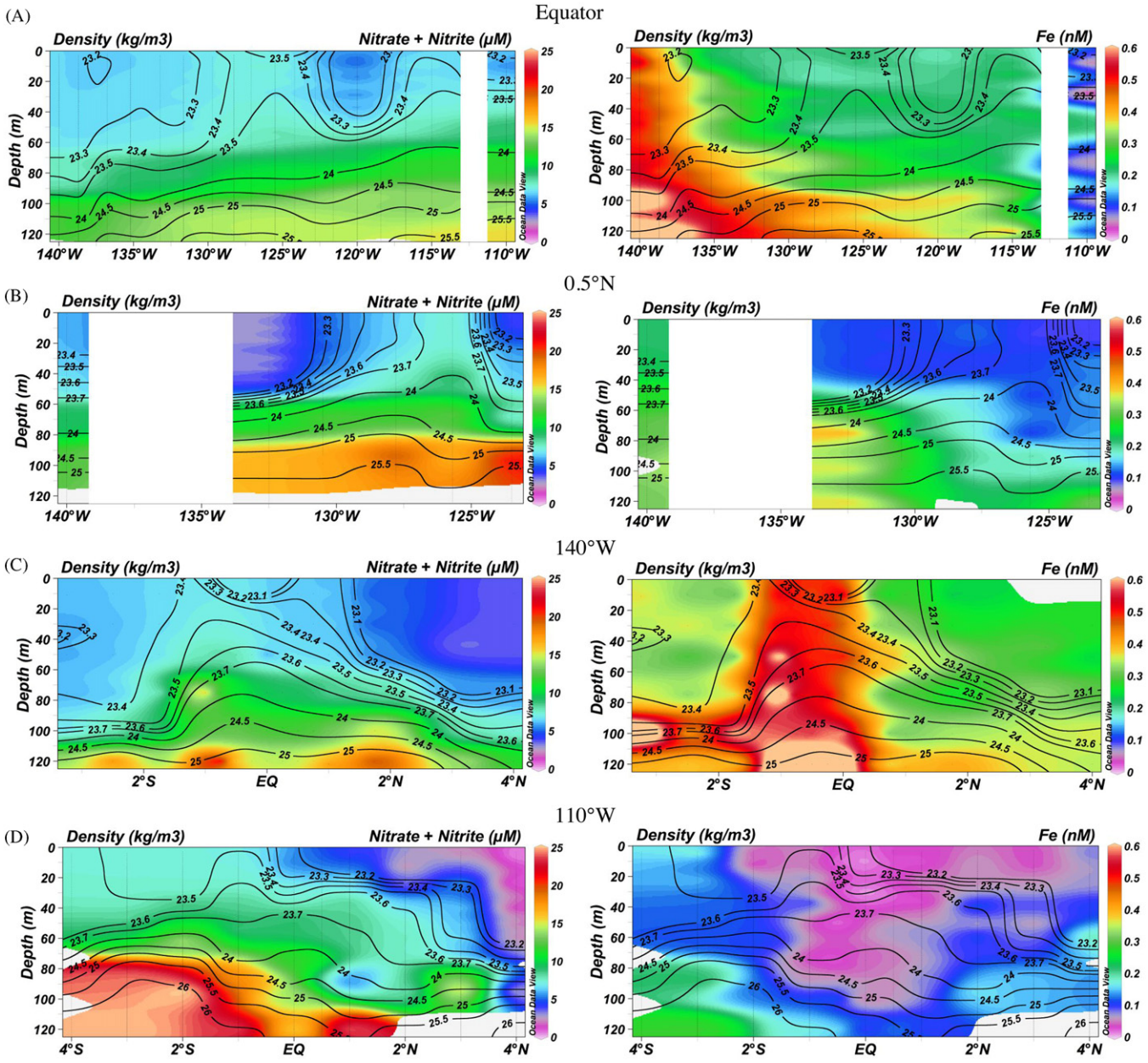

Fig. 3. Contour plots of Nitrate+Nitrite (μM) and dissolved Fe (nM) data are shown, arranged by transect. Overlain on these plots are density (kg/m^3) contours. Blank areas of the figures denote an absence of data for that area.

the euphotic zone, whereas silicic acid varied from 0.2 to 18.7 μM (Dugdale et al., 2011).

Density contour lines (sigma-t, kg m^{-3}) on the N+N maps can be used to locate upwelling regions. For instance, on the equatorial transect (EB04) between 130°W and ~122°W, as well as at ~115°W, the 23.5 kg m^{-3} isopycnal rises from 60 to ~20 m. Similarly, the 23.5 kg m^{-3} isopycnal shoals from ~60 m to the surface between 131 and 124°W on the 0.5°N transect (EB05). The strong meridional flows in ADCP current velocity (Fig. 2) suggest that these areas were affected by the passage of tropical instability waves. The meridional transect at 140°W also shows distinct upwelling (23.1-23.4 kg m^{-3} isopycnals) between 2°S and 2°N, with the 23.5 kg m^{-3} isopycnal rising from 110 m at 2°S to ~35 m at 1°S. The 110°W transect indicates a more limited latitudinal range of upwelling between the equator and 2°S, with the 23.5 kg m^{-3} isopycnal reaching the surface at 1°S.

3.3. Dissolved iron

Dissolved iron (hereafter referred to as Fe) ranged from undetectable (limit of detection: 0.08 nM) to 0.6 nM in the euphotic zone and showed a very different distributional pattern over the study area compared to N+N (Fig. 3, right panels). On the equatorial transect, Fe values were highest (> 0.34 nM) in surface waters at 140°W and 138.7°W, increasing to ~ 1 nM at 120 m (Fig. 3A). Fe became progressively more depleted throughout the upper 200 m to the east. By 110°W, Fe was undetectable in the upper 100 m, and only 0.18-0.37 nM from 140 to 200 m (data not shown). The 0.5°N zonal transect showed a similar decreasing trend to the east, but Fe levels were lower overall because this transect was at the northern boundary of the EUC (Fig. 3B). At 140°W, Fe concentrations were 0.2 nM at the surface, and only 0.5 nM at 200 m Fe (data not shown). This transect did not extend

as far east as the equatorial transect, and Fe was always above the detection limit of 0.08 nM in surface waters, albeit only slightly higher (0.09-0.11 nM) from 130°W to 123.4°W.

Fe concentrations along the meridional 140°W transect were quite high in the region of the EUC from 1°S to 0° (Fig. 3C, ~0.5 nM in surface samples, increasing to 0.8 nM at 120 m). Fe concentrations were lower polewards of the equator, increasing from 0.2-0.3 nM at the surface to ~0.6 nM at 120 m. In contrast, the meridional transect at 110°W showed undetectable Fe in the upper 100 m between 1°S and 1°N and moderate concentrations from 150-200 m (~0.3 nM, data not shown) (Fig. 3D). Polewards of these latitudes at 110°W, 0.1-0.2 nM Fe occurred all the way to the surface at 3°S, and 0.1 nM concentrations were found as shallow as 60 m at 2°S and 2°N and 40 m at 4°N.

3.4. Pigment composition and depth profiles

The composition of major accessory pigments relative to TChl*a* or MVChl*a* was relatively invariant (Table 1). MVChl*a* and DVChl*a* comprised 63.5% (range: 60.8-65.3%) and 36.4% (range: 34.4-39.2%), respectively, of TChl*a*. ZEAX was 23.7% of TChl*a* (range: 22.6-25.2%). The pigments HEX, BUT, FUCO and PER averaged 46.3, 22.6, 7.8 and 3.0% of MVChl*a*, respectively. However, MVChl*a* was a significantly lower percentage of TChl*a* ($Q=4.0$, $P<0.001$) and DVChl*a* was a significantly higher percentage of TChl*a* ($Q=4.2$, $P<0.001$) on the EB04 equatorial transect relative to the other transects. In addition, relative to the other transects, the percent of FUCO relative to MVChl*a* was significantly higher on the EB05 0.5°N transect ($Q=5.0$, $P<0.001$).

Mean (± 1 std dev) depth profiles of pigment are compared among transects in Fig. 4. Mixed-layer concentrations of pigments were lower along 110°W, with TChl*a* averaging 38% less than on the other three transects (178 ± 21 ng L^{-1} versus 264-314 ng L^{-1}), and other pigments were also proportionately lower. ZEAX declined with depth in all transects. HEX showed subsurface maxima at the 5% light level on all transects, co-occurring with a subsurface FUCO maxima along the equator and at 110°W. Subsurface maxima for FUCO were somewhat shallower, at the 8% light level, along the 0.5°N transect and at 140°W. In contrast, BUT maxima were deeper, at the 0.8% light level. Generally, PER declined with depth, but at 110°W a slight subsurface maximum occurred at the same light level as HEX and FUCO.

3.5. Depth-integrated pigments

Depth-integrated values of pigments for the euphotic zone are arranged by cruise, transect and station in Table 2. The main feature of interest on the EB04 equatorial transect is the substantial eastward decline of prokaryote-associated pigments, DVChl*a* and ZEAX, while MVChl*a* and eukaryote-associated pigments remained relatively similar on either side of the declining west-to-east Fe gradient. DVChl*a* and ZEAX each decreased by about half, from 14.8 to 8.6 μg m^{-2} and from 8.0 to 4.2 μg m^{-2}, respectively, between 140 and 110°W. The corresponding decrease in depth-integrated TChl*a*, from 32 to 25 μg m^{-2}, reflects principally the decrease in DVChl*a*. MVChl*a* was slightly lower at 110°W (16.4 μg m^{-2}) compared to 140°W (17.2 μg m^{-2}), but a transect low concentration (12.0 μg m^{-2}) occurred in the anomalous area of westward surface currents and low mixed-layer macronutrient at 120°W. HEX, FUCO and PER, all representing eukaryotic populations with MVChl*a*, also did not decline appreciably across the transect, and HEX and FUCO had their lowest values at 120°W.

The highest pigment values on the 0.5°N transect (EB05) occurred at 127.8°W and 125.7°W. These are locations where subsurface eastward current velocities were highest, indicating the core of the EUC, and where high meridional velocities suggested TIW activity (Table 2). Elsewhere, no discernible E-W trends in pigment concentrations were seen on this transect. However, the EB05 zonal transect did not go as far eastward as EB04.

The meridional transect at 140°W showed the highest pigment concentrations for TChl*a*, DVChl*a* and ZEAX (32.7 ± 1.4, 13.0 ± 1.4, and 7.9 ± 0.3 μg m^{-2}, respectively) from 0 to 1°S, the core of equatorial upwelling (Table 2). DVChl*a* and ZEAX were lowest at 1°N (6.2 and 4.0 μg m^{-2}, respectively), whereas other pigments had transect minimum values at 2.5°N (TChl*a*, MVChl*a*, HEX, BUT and FUCO were 22-37% lower there than at other stations). 1°N was the northern edge of the Fe gradient from the EUC and was characterized by strong meridional (southward) and zonal (eastward) current flow. 2.5°N was the southern edge of the area away from the equator with a subsurface Fe maximum and was characterized by little meridional current flow. PER concentrations were approximately the same across the transect (average 0.5 ± 0.1 μg m^{-2}).

DVChl*a* was fairly constant across the EB04 transect at 110°W (average 8.3 ± 0.5 μg m^{-2}). Except for lower values at 3°S and 4°N, TChl*a*, MVChl*a*, HEX and BUT concentrations were also relatively invariant across this transect (25.7 ± 1.6, 17.2 ± 1.4, 7.8 ± 0.7, 4.2 ± 0.7 μg m^{-2}, respectively). ZEAX was lowest in the equatorial region (1°S-0°) and higher at 4°S, whereas FUCO was high from 1°S-3°N (42% higher there than at other stations). PER was elevated away from the equator at 110°W, with highest integrated values at 4°S and 3°N.

Comparing the two zonal transects, by averaging all comparable stations longitudinally between 122.8 and 140°W (7 stations at the equator and 6 stations at 0.5°N), reveals the same mean integrated TChl*a* concentrations for both equator and 0.5°N stations (28.5 μg m^{-2}), and similar concentrations of MVChl*a* (16.9 and 18.5 μg m^{-2}, respectively) and DVChl*a* (11.6 and 10.9 μg m^{-2}, respectively). Transect means of all other measured pigments were within 15% of each other, and none of the differences were significant (two-tailed t-test, $P \geq 0.10$).

For meridional transects at 110 and 140°W, depth-integrated pigment averages were not significantly different at the 90% confidence level. However, for pair-wise comparisons at each light level (data not shown), transect-mean values were significantly

Table 1
Relative abundance of major pigments relative to TChl*a* or MV*Chla*. Shown are percents of MVChl*a* (MV), DVChl*a* (DV), and ZEAX relative to TCHL*a*, as well HEX, BUT, FUCO, and PER relative to MVChl*a*. All pigments are depth-integrated averages for the euphotic zone. Data are averages ± 1 standard deviation arranged by transect and cruise. The number of observations is shown after each transect designation.

CRUISE	TRANSECT	MV	DV	ZEAX	HEX	BUT	FUCO	PER
EB04	0°, n=88	60.8 ± 8.8	39.2 ± 8.8	23.3 ± 10.5	48.0 ± 4.4	22.4 ± 5.1	7.9 ± 1.9	2.9 ± 0.9
EB04	110°W, n=72	65.3 ± 7.3	34.4 ± 6.8	25.2 ± 13.0	46.7 ± 4.6	20.9 ± 8.1	7.8 ± 1.9	3.1 ± 1.0
EB05	0.5°N, n=48	64.2 ± 8.9	35.8 ± 8.9	22.6 ± 11.0	43.8 ± 5.3	24.0 ± 5.3	8.9 ± 2.3	2.8 ± 1.1
EB05	140°W, n=64	64.7 ± 10.4	35.3 ± 10.4	23.4 ± 11.2	45.2 ± 3.6	23.5 ± 5.3	6.9 ± 1.4	3.2 ± 1.0
Overall	**N=272**	**63.5 ± 9.0**	**36.4 ± 8.9**	**23.7 ± 11.4**	**46.3 ± 4.7**	**22.6 ± 6.2**	**7.8 ± 2.0**	**3.0 ± 1.0**

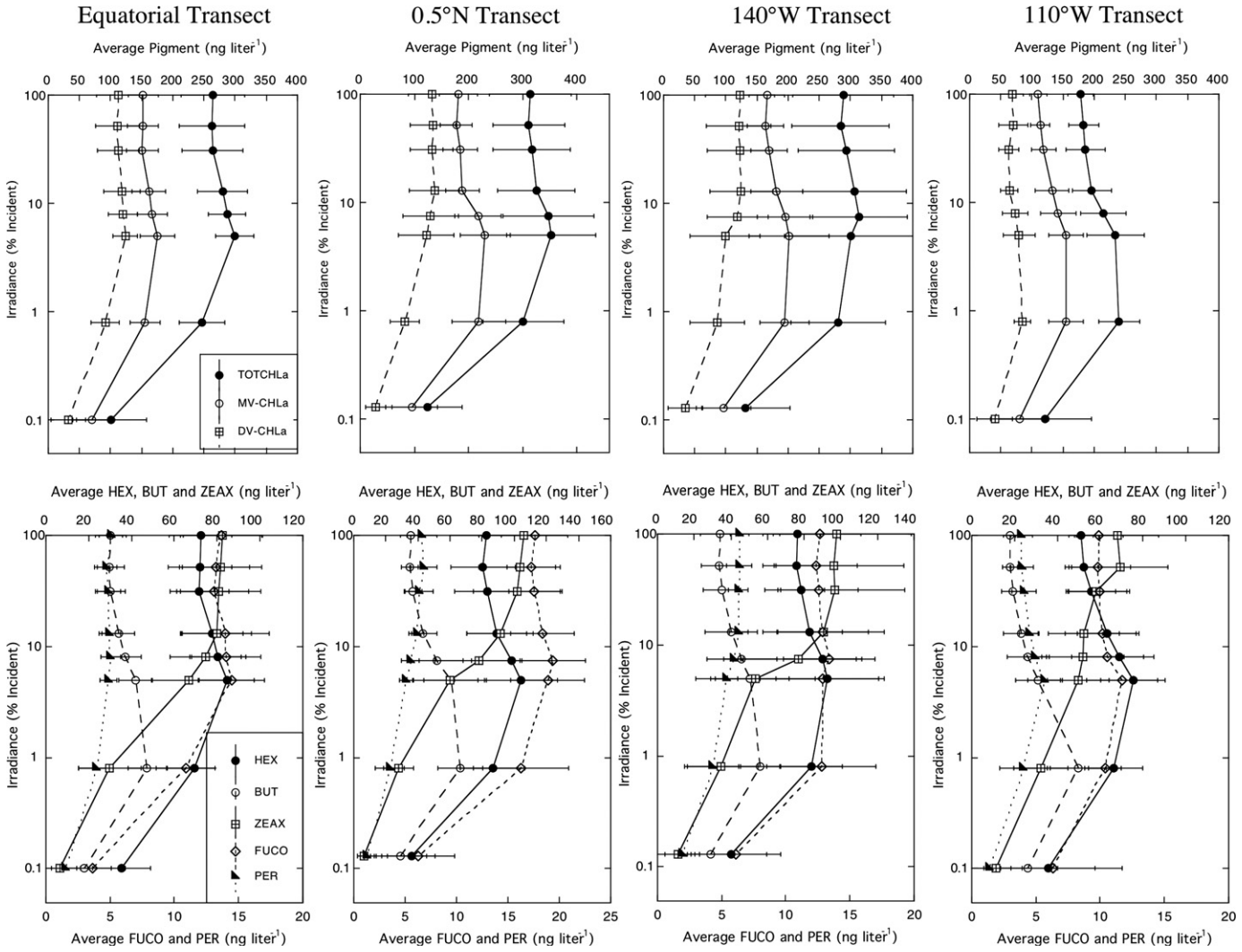

Fig. 4. Depth profiles of pigment concentrations, plotted by transect. All stations on each transect were combined to generate averages (± one standard deviation of the mean). The upper figures show the distributions of TChl*a*, MVChl*a*, and DVChl*a*. The lower figures show HEX, BUT, ZEAX, FUCO and PER distributions. Note that FUCO and PER are plotted on a separate axis than HEX, BUT and ZEAX, due to their much smaller magnitude.

lower at 110°W relative to 140°W from the surface to the 8% light level (2-tailed t-test, $P < 0.10$). At the 5% light level, all pigments were the same between the two transects, with the exception of BUT (which was still significantly lower). MVChl*a* and HEX were significantly lower at 110°W than 140°W at the 0.8% light level. There were no significant pigments differences at the 0.1% light level.

3.6. *Phytoplankton rates from microscopy, flow cytometry and HPLC pigments*

To evaluate whether our pigment-corrected rates adequately represent true cellular growth rates, we compare pigment and microscopy-based estimates from EB05 (a full complement of microscopy-based biomass data for initial and final samples were not available for EB04). Phytoplankton community rates are compared for total autotroph biomass versus TChl*a*-based estimates, and diatom biomass rates are compared with FUCO-based estimates. Further comparisons are also made between rate estimates from DVChl*a* versus FCM cell counts of *Prochlorococcus*.

The pigment-microscopy comparison shows that the community grew at a high rate (0.7-0.8 d^{-1}) down to the 13% light level, with rates declining to $\sim$0.2 d^{-1} at the 1% and 0.1% light levels (Table 3). Diatoms showed a similar trend, but high-light growth rates were double those for the full community (1.4-1.8 d^{-1}) and negative rates (-0.5 to -0.8 d^{-1}) were found at the base of the euphotic zone. Mean growth estimates from pigments and microscopy showed extremely good agreement. However, because the volumes analyzed for microscopy were small (only a small fraction of the 50-500 ml samples is examined) compared to the 2-L HPLC pigment analyses, the approaches were quite different in terms of variability of the resulting rate estimates.

Unlike other taxa, the rate estimates for *Prochlorococcus* were slightly different between our two cruises (Fig. 5). For both cruises, growth rates ranged from 0.3 to 0.7 d^{-1} at the 5-50% light levels and declined to $\sim$0.1 d^{-1} at the base of the euphotic zone. The pigment and FCM approaches gave remarkably similar results, especially for EB04. For EB05, DVChl*a* estimates of growth rates were slightly higher than cell-based estimates in the surface and mid-euphotic zone, and slightly lower at the base of the euphotic zone. Nevertheless, the overall similarity between the two methods strongly suggests that the rate correction applied to the pigment data (changes in FCM red fluorescence per cell) did a generally good job in accounting for cellular changes in DVChl*a* during the incubations. Net growth rates were essentially zero for

Table 2
Depth-integrated pigment concentrations ($\mu g\, m^{-2}$) for each station of each transect, as well as the mean depth-integrated pigment concentrations for each transect.

Longitude	TChl*a*	MVChl*a*	DVChl*a*	ZEAX	HEX	BUT	FUCO	PER
EB04, Equatorial (0°) Transect								
140°W	32.05	17.23	14.82	7.99	8.57	4.00	1.50	0.55
138.68°W	30.16	16.05	14.11	8.00	8.04	3.86	1.36	0.47
135.2°W	31.98	19.52	12.47	5.98	9.77	5.06	1.40	0.41
131.64°W	25.59	14.94	10.65	5.94	7.12	3.51	1.10	0.54
128.26°W	26.04	15.34	10.70	5.64	6.97	3.77	1.34	0.43
125.5°W	28.02	19.93	8.09	4.27	9.05	4.83	1.83	0.45
122.8°W	25.85	15.28	10.57	6.16	6.76	3.69	1.07	0.50
120°W	20.33	12.01	8.31	4.57	5.46	3.18	0.90	0.44
116.74°W	26.95	18.20	8.75	6.00	8.04	4.40	1.21	0.39
110°W	24.92	16.37	8.55	4.21	7.60	4.04	1.22	0.44
Average	**27.19**	**16.49**	**10.70**	**5.88**	**7.74**	**4.03**	**1.29**	**0.46**
EB05, 0.5°N Transect								
140°W	25.00	17.64	7.35	4.68	8.06	4.82	1.11	0.41
132.5°W	23.67	15.60	8.07	5.06	6.98	4.00	1.51	0.44
130.5°W	26.57	17.28	9.30	5.18	6.36	4.89	1.50	0.41
127.8°W	32.86	20.96	11.90	6.69	9.24	5.09	1.62	0.50
125.7°W	38.48	23.22	15.26	7.68	9.77	6.04	1.98	0.43
123.5°W	24.61	16.62	7.99	5.11	7.60	3.79	1.62	0.51
Average	**28.53**	**18.55**	**9.98**	**5.73**	**8.00**	**4.77**	**1.56**	**0.45**
EB05, 140°W Transect								
Latitude								
4°N	25.36	16.03	9.33	6.29	7.83	3.53	0.73	0.63
2.5°N	22.47	14.22	8.25	5.15	6.31	2.95	0.83	0.52
1°N	25.80	19.63	6.17	4.04	9.59	5.07	1.46	0.61
0.5°N	25.00	17.64	7.35	4.68	8.06	4.82	1.11	0.41
0°	31.15	19.50	11.65	7.94	8.36	5.09	1.36	0.48
0.5°S	33.17	20.25	12.93	7.58	8.60	5.27	1.47	0.50
1°S	33.75	19.26	14.49	8.17	8.08	5.08	1.42	0.51
2.5°S	26.48	16.80	9.68	5.21	7.73	3.84	1.29	0.57
Average	**27.90**	**17.92**	**9.98**	**6.13**	**8.07**	**4.46**	**1.21**	**0.53**
EB04, 110°W Transect								
4°N	17.72	9.84	7.57	5.41	4.67	1.87	0.92	0.34
3°N	27.11	18.82	8.29	5.11	8.62	4.65	1.53	0.62
2°N	28.09	19.25	8.85	5.03	9.04	4.65	1.39	0.48
1°N	26.59	17.61	8.98	5.04	7.97	4.73	1.32	0.51
0°	24.92	16.37	8.55	4.21	7.60	4.04	1.22	0.44
1°S	24.76	16.64	8.12	4.18	7.25	4.77	1.38	0.50
2°S	25.29	16.36	8.92	5.60	7.08	3.63	0.98	0.51
3°S	20.40	12.50	7.90	5.52	6.02	2.95	0.89	0.37
4°S	23.44	15.57	7.87	6.23	7.40	2.89	1.04	0.61
Average	**24.26**	**15.88**	**8.34**	**5.15**	**7.29**	**3.80**	**1.19**	**0.49**

Table 3
Comparison of microscopical- and pigment-based growth and net growth rates. Cell-based net growth rates (k) were calculated as the natural log of the ratio of the final to initial values of the microscopy-estimated carbon biomass of the appropriate phytoplankton populations. Cell-based growth rates (μ) were calculated as the sum of the cell-based net growth and mortality rates (i.e., $k + m$) derived from the seawater dilution experiments. Pigment-based rates (TChl*a* and FUCO) were calculated as described in the text, with corrections for unbalanced pigment acclimation. All data are averages ± 1 standard deviation of the mean.

Phytoplankton community growth rates			
%Irradiance	**Cell-based *k***	**Cell-based *μ***	**TChl*a*-based *μ***
100	0.12 ± 0.40	0.68 ± 0.39	0.69 ± 0.31
52	0.24 ± 0.36	0.84 ± 0.39	0.78 ± 0.23
31	0.13 ± 0.26	0.71 ± 0.25	0.70 ± 0.19
13	0.31 ± 0.37	0.88 ± 0.32	0.81 ± 0.20
8	0.14 ± 0.51	0.53 ± 0.48	0.52 ± 0.13
5	0.21 ± 0.23	0.52 ± 0.29	0.48 ± 0.18
0.8	0.01 ± 0.27	0.16 ± 0.25	0.15 ± 0.19
0.1	0.25 ± 0.57	0.27 ± 0.53	0.21 ± 0.09
Diatom community growth rates			
%Irradiance	**Cell-based *k***	**Cell-based *μ***	**FUCO-based *μ***
100	1.09 ± 1.2	1.82 ± 1.11	1.76 ± 0.36
52	1.00 ± 1.2	1.87 ± 1.11	1.60 ± 0.15
31	0.76 ± 1.1	1.61 ± 0.99	1.50 ± 0.08
13	0.58 ± 0.9	1.45 ± 0.97	1.36 ± 0.23
8	−0.10 ± 1.2	0.45 ± 1.18	0.56 ± 0.15
5	0.13 ± 1.5	0.63 ± 1.53	0.63 ± 0.15
0.8	−0.78 ± 1.2	−0.54 ± 1.09	−0.54 ± 0.25
0.1	−0.81 ± 0.7	−0.83 ± 0.80	−0.78 ± 0.21

both cruises ($-0.05\ d^{-1}$ for cell-based rates, excluding 100% I_o), and strongly negative (approx. $-1.0\ d^{-1}$, Fig. 5) for incubation bottles held unnaturally for 24 h at 100% I_o.

3.7. Taxon-specific growth rates of phytoplankton

Given the good agreement between pigment-based rates and those from FCM or microscopy, the lower variance associated with HPLC rates, and the rate similarities between transects and cruises at each light level, we present pigment-based estimates of growth (μ) and net growth (k) rates in Fig. 6 as two-cruise averages. As indicated above, the rates were not uniform with depth, but can be divided into three depth zones, here designated as the surface mixed layer (13-100% light levels), the mid-euphotic zone (5-8% light level), and the base of the euphotic zone (0.1-1% light level). Mixed-layer rates can be divided further to account for the anomalously low rates in bottles incubated at 100% of incident surface irradiance. For TChl*a* and MVChl*a*, for example, surface rates of 0.5 and $0.6\ d^{-1}$, respectively, were 60-70% of the mean rates at 50, 30 and 13% light levels (TChl*a* = $0.81 \pm 0.05\ d^{-1}$ and MVChl*a* = $0.86 \pm 0.04\ d^{-1}$). As previously noted, the high-light depression of growth rate was even greater for DVChl*a*, with a negative surface rate ($-0.4\ d^{-1}$) compared to nearly one doubling per day ($0.63 \pm 0.13\ d^{-1}$) deeper in the mixed layer. Surface ZEAX rates ($0.15\ d^{-1}$) were also much lower than the $0.74 \pm 0.07\ d^{-1}$ average for the 50-30-13% light levels. In contrast, growth rates for eukaryote populations were not depressed at the surface, with surface mixed-layer (including the 100% light level) averaging $1.60 \pm 0.09\ d^{-1}$ for FUCO, $0.71 \pm \pm 0.07\ d^{-1}$ for HEX, $1.03 \pm 0.08\ d^{-1}$ for BUT, and $0.40 \pm 0.09\ d^{-1}$ for PER.

With the exception of PER, which increased by 50% to $0.59 \pm 0.20\ d^{-1}$, growth rates dropped in the mid-euphotic zone (8-10% light level), most dramatically for FUCO. FUCO rates at these light levels averaged $0.59 \pm 0.06\ d^{-1}$, a decrease of $1\ d^{-1}$ relative to surface values. Mid-euphotic zone growth rates for TChl*a*, MVChl*a*, DVChl*a* and HEX were approximately $0.5\ d^{-1}$, whereas ZEAX and BUT decreased to $0.64\ d^{-1}$ and $0.76 \pm 0.15\ d^{-1}$, respectively.

Growth rates were further depressed at the base of the euphotic zone, again with the exception of PER, which was the same at these depths ($0.38 \pm 0.31\ d^{-1}$) as in the surface mixed layer. This could be indicative of a widespread mixotrophic nutritional strategy among pigmented dinoflagellates (reviewed by Stoecker, 1999), which would make their growth rates less dependent on photosynthesis and light. Mean growth rates for TChl*a*, MVChl*a*, ZEAX and BUT were 0.23-0.28 d^{-1} in the lower euphotic zone, HEX was $0.14\ d^{-1}$, DVChl*a* was $-0.01\ d^{-1}$, whereas FUCO rates were highly negative at $-0.63\ d^{-1}$ (also evident in microscopical analyses). Negative FUCO growth rates could indicate a population of largely senescing diatoms at the base of the euphotic zone.

The difference in temperature between the surface (where cooling water to the incubators was obtained) and the 5% light depth for all stations on both cruises was only ≤ 1°C (data not shown). However, larger differences in temperature existed between

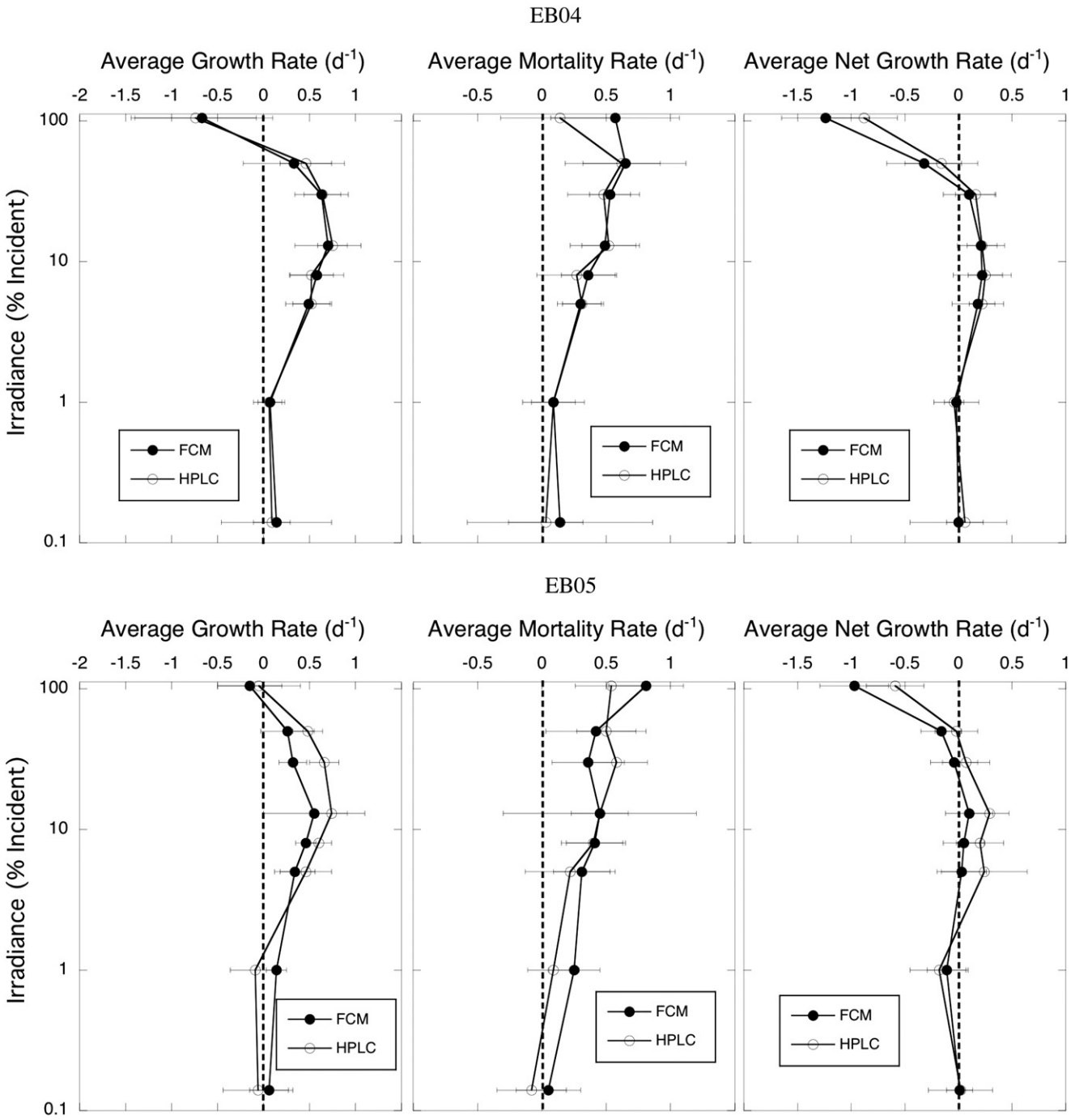

Fig. 5. *Prochlorococcus* rates (growth rate, mortality rate, and net growth rates) plotted by light level, comparing two analysis methods: flow cytometry (FCM) and high performance liquid chromatography (HPLC). The data were combined for all stations on each cruise to generate averages ± 1 standard deviation of the mean. The top panels show EB04 rates, and the bottom panels show EB05 rates.

the base of the euphotic zone (0.1 – 0.8% light levels) relative to the surface waters. For instance, up to a 10°C difference in temperature was found along the 110°W transect on EB04 when comparing the 0.1% light level to the surface. Thus, the samples from the 0.1% light level experienced temperatures that potentially could have nearly doubled their maximum growth rates, if we use the Eppley curve as a guide (Eppley, 1972). For the 8% light level along this transect, the difference in temperature was ~4°C relative to the surface – which would potentially increase growth rates by 30%. The other 3 transects showed smaller differences between the 0.1% light level and the surface, ranging between 4-7°C – which corresponds to a potential increase in growth rates of 30-60%. If just the 0.8% light level and shallower depths are considered, the difference was always 3°C or less, which corresponds to a potential increase in growth of less than 20%. Since estimated growth rates at the 0.1% and 0.8% light depths were low, and sometimes even negative, the temperature effect was likely not the most important variable governing growth rates at the base of the euphotic zone.

A comparison of all taxon-specific growth rates for both cruises from combined surface mixed-layer samples revealed that diatom growth rates were significantly higher relative to all other taxa, whether considering each cruise separately or combining the data for both cruises (Tukey test, $P=0.005$). The second highest growth rates were found for pelagophytes, followed by prymesiophytes.

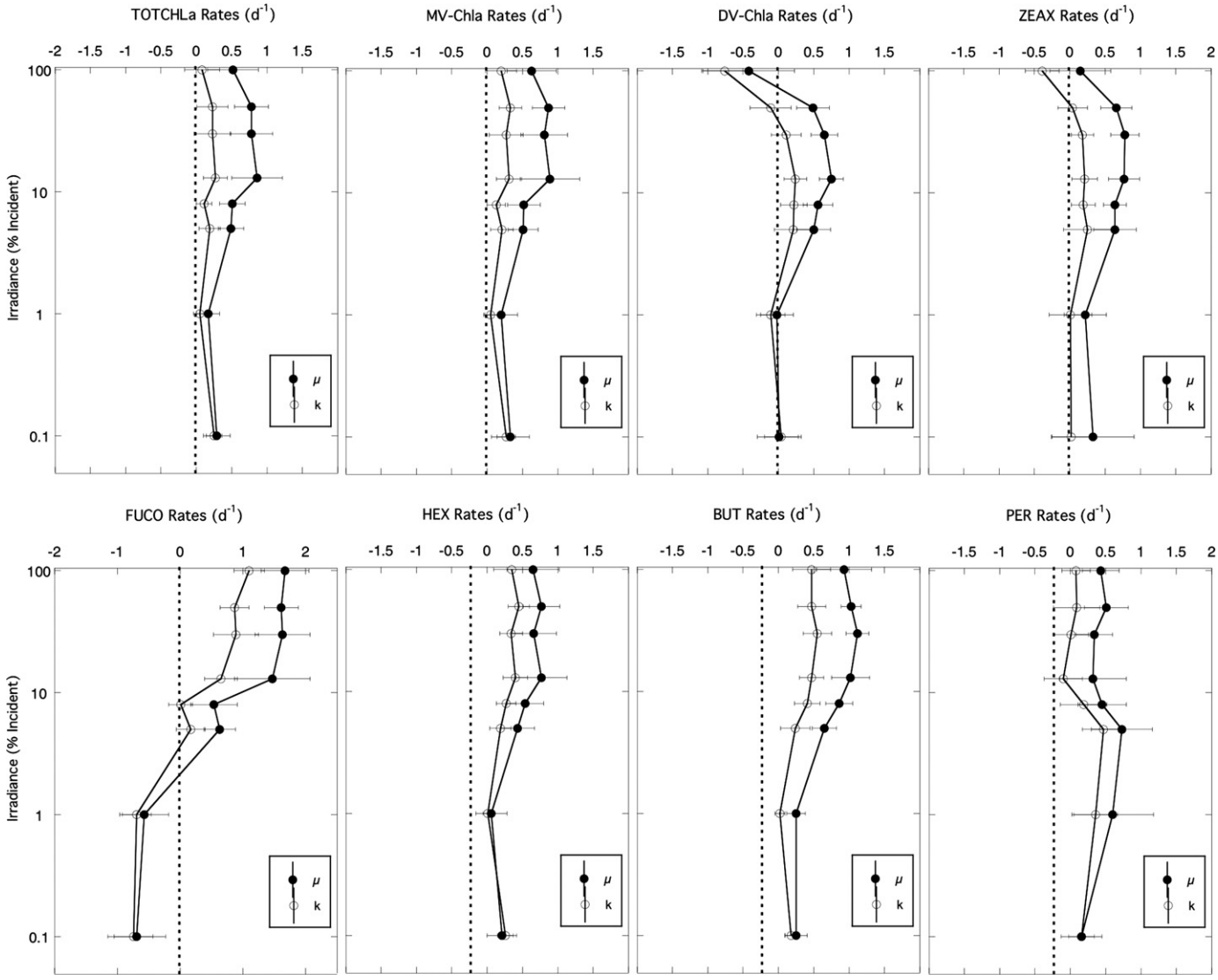

Fig. 6. Pigment-based gross (μ) and net (k) growth rates (d^{-1}), plotted as a function of light level. Data were combined from all stations on both cruises to generate averages (± 1 standard deviation of the mean). Light levels are plotted as the percent of incident irradiance. The top panels are of rates of TChl*a*, MVChl*a*, DVChl*a* and ZEAX, whereas the bottom panels are of FUCO, HEX, BUT and PER.

Growth rates of prokaryotic taxa, as indicated by DVChl*a*, as well as by cell abundances of SYN and PRO, were always significantly lower than eukaryotic rates, with the exception of dinoflagellate growth rates based on PER, which were the lowest rates measured. Net growth rates ($k=\mu-m$) showed that microzooplankton grazing consumed most of the growth of the phytoplankton community, leaving $0.18 \pm 0.08\ d^{-1}$ net growth for TChl*a* and similar values for MVChl*a* ($0.22 \pm 0.09\ d^{-1}$) and PER ($0.16 \pm 0.18\ d^{-1}$). FUCO, HEX and BUT showed the highest net growth, at $\sim 0.3\ d^{-1}$. In contrast to eukaryotes, essentially all of the growth of prokaryotic autotrophs was consumed by microzooplankton, with an average net growth rate of $-0.02\ d^{-1}$ for DVChl*a* and $0.06\ d^{-1}$ for ZEAX. Thus, in accord with previous observations and predictions (e.g., Landry et al., 1997), the standing stocks of prokaryotic picoplankton were held in check by micrograzers.

3.8. *Pigment and rate distributions along the EB04 equatorial transect*

Distributions of pigment standing stocks, growth and net growth rates along the EB04 equatorial transect are presented in Figs. 7 and 8. Other transects are not shown because the trends were similar to the equatorial transect or were adequately described from the depth-integrated patterns (Table 2). For the major pigments of eukaryotic phytoplankton, MVChl*a*, HEX, BUT, FUCO and PER, the equatorial contour plots illustrate that the relative constancy of depth-integrated pigment values in Table 2 is the result of two opposing trends. Surface mixed-layer concentrations decreased to the east with the declining Fe gradient (Fig. 7). The magnitudes of subsurface pigment maxima, however, increased to the east. Highest concentrations of BUT (2- to 3-fold higher than surface values) were found at the 0.8% light level, which was deeper than the maxima for other pigments (usually the 5% I_o).

TChl*a*-based growth rates do not show a pronounced eastward decline, but the location of maximum growth shoaled slightly from west to east (Fig. 7). Net growth rates were also relatively constant across the transect. FUCO standing stock and rate data showed similar patterns. HEX and BUT showed the same overall trends, with positive net growth rates extending from west to east; however, net growth rates for these populations were essentially zero below the surface mixed layer.

Cell abundances of the phototrophic bacteria, *Prochlorococcus* and *Synechococcus*, were distributed similarly across the equatorial

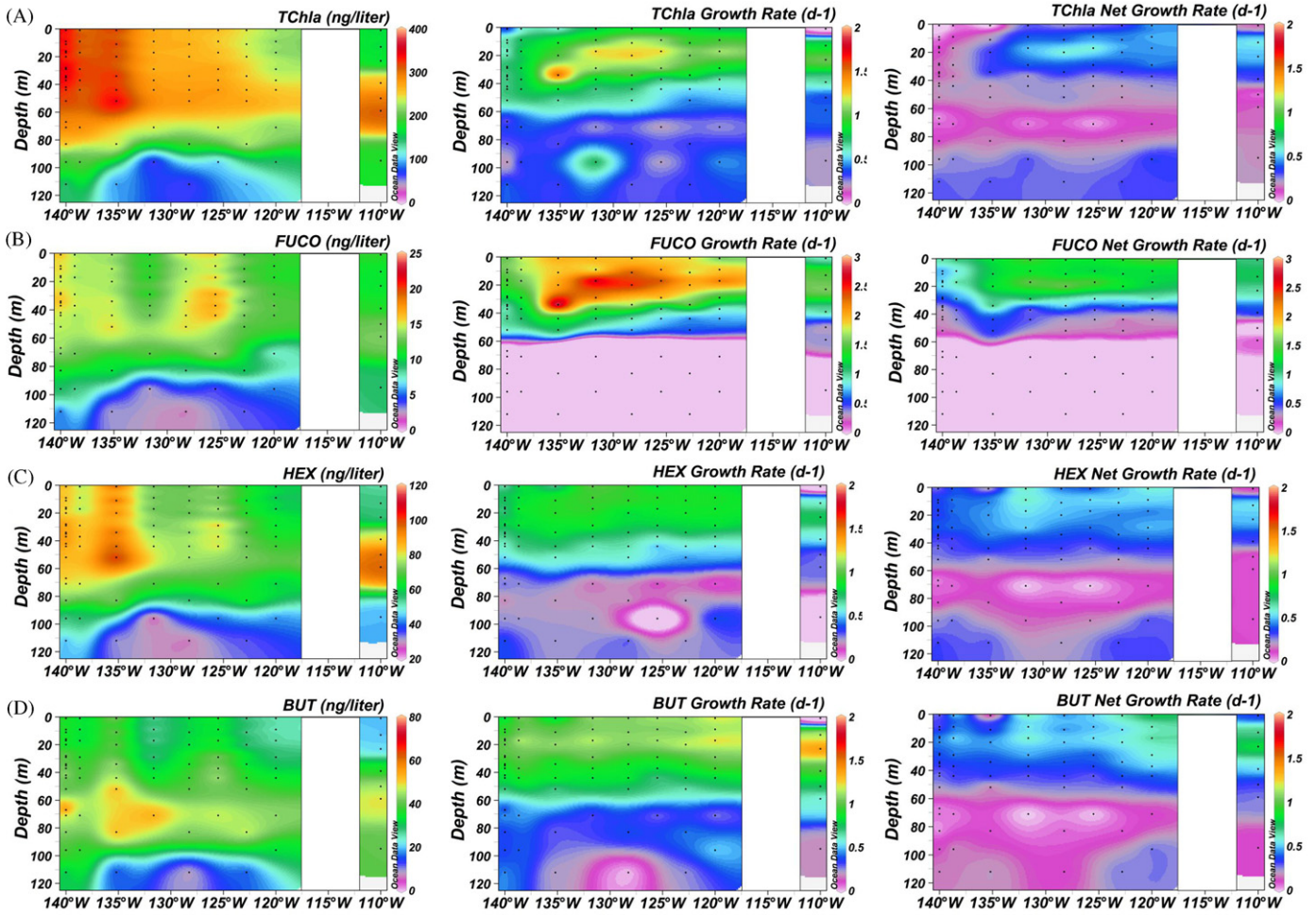

Fig. 7. Contour plots of eukaryotic pigment stocks and rates for the equatorial transect. Shown are the standing stocks of TChl*a*, FUCO, HEX and BUT, as well as their growth rates (μ) and net growth rates (k). Three panels are shown for each parameter, with the left-most panel showing the standing stock, the middle panel showing the growth rates, and the right-most panel showing the net growth rates. From top to bottom, the panels are arranged as follows: A) TChla, B) FUCO, C) HEX, D) BUT. Blank areas denote an absence of data.

transect, but *Prochlorococcus* was always ≥ 10-fold more abundant (Fig. 8). Cell abundances of both populations, as well as indicator pigments DVChl*a* and ZEAX, decreased from west to east, following the Fe gradient. DVChl*a* showed a subsurface maxima across the transect, usually at the 5% I_o light depth (Fig. 8). However, these deep DVChl*a* maxima became more prominent toward the east, with only a slight (< 10% elevation at depth) subsurface maxima from 125 to 140°W, but pronounced maxima (10 - 120% higher than the surface) from 110 to 123°W. In addition, consistent with its photoprotective role, ZEAX concentrations were typically highest at the surface decreasing with depth, except for subsurface maxima at ~40 m at the eastern end of the transect (110 and 116.7°W).

Overall, growth rates of prokaryotic autotrophs did not decrease to the east (Fig. 8). However, the highest growth rates of DVChl*a* shifted from the near surface at 140 to 120°W to deeper at 110°W. This was also true for *Prochlorococcus* cell-based rates. *Synechococcus* growth rates showed a similar pattern to *Prochlorococcus*, except they were near zero at 120°W. As noted above for *Prochlorococcus* depth profiles (Figs. 5 and 6), net growth rates of prokaryotes were near zero throughout the water column, for both the pigment and cell-based measurements (Fig. 8).

No statistically significant differences were found for taxon-specific growth rates between cruises, or between upwelling and non-upwelling zones (t-test, P=0.001). In terms of spatial differences in rates between 110°W and 140°W, only HEX ($0.44 \pm 0.48\ d^{-1}$, n=36, and $0.73 \pm 0.13\ d^{-1}$, n=40, respectively) and PER ($0.46 \pm 0.47\ d^{-1}$, n=30, and $0.33 \pm 0.19\ d^{-1}$, n=40) showed a significant difference between means at these locations (t-test, P=0.001), with HEX having higher rates at 140°W, but PER having higher rates at 110°W.

3.9. Euphotic-zone estimates of growth and production rates

Depth-averaged rates of phytoplankton growth and net growth are given in Table 4. Community growth rates (TChl*a*) averaged $0.53 \pm 0.17\ d^{-1}$ for all stations on both cruises, with little difference between cruises ($0.54 \pm 0.20\ d^{-1}$ on EB04 *versus* $0.51 \pm 0.12\ d^{-1}$ on EB05). If just autotrophic eukaryotes and *Synechococcus* are considered (MVChl*a*), growth rates were slightly higher on average ($0.57 \pm 0.20\ d^{-1}$). In contrast, the depth-averaged growth rate of *Prochlorococcus* (DVChl*a*) was lower overall, at $0.34 \pm 0.14\ d^{-1}$, while mean ZEAX growth, representing both *Prochlorococcus* and *Synechococcus*, was intermediate ($0.54 \pm 0.14\ d^{-1}$). Prymnesiophyte growth rate (HEX=$0.46 \pm 0.23\ d^{-1}$) was similar to the overall community, while diatom (FUCO=$0.86 \pm 0.32\ d^{-1}$) and pelagophyte (BUT=$0.69 \pm 0.10\ d^{-1}$) growth rates were higher than the community average.

Net growth rates for the total community (TChl*a*) were $0.16 \pm 0.11\ d^{-1}$, with net growth for EB04 somewhat higher than for EB05 ($0.20 \pm 0.09\ d^{-1}$ *versus* $0.12 \pm 0.12\ d^{-1}$; Table 4). Net growth rates for the MVChl*a* portion of the community

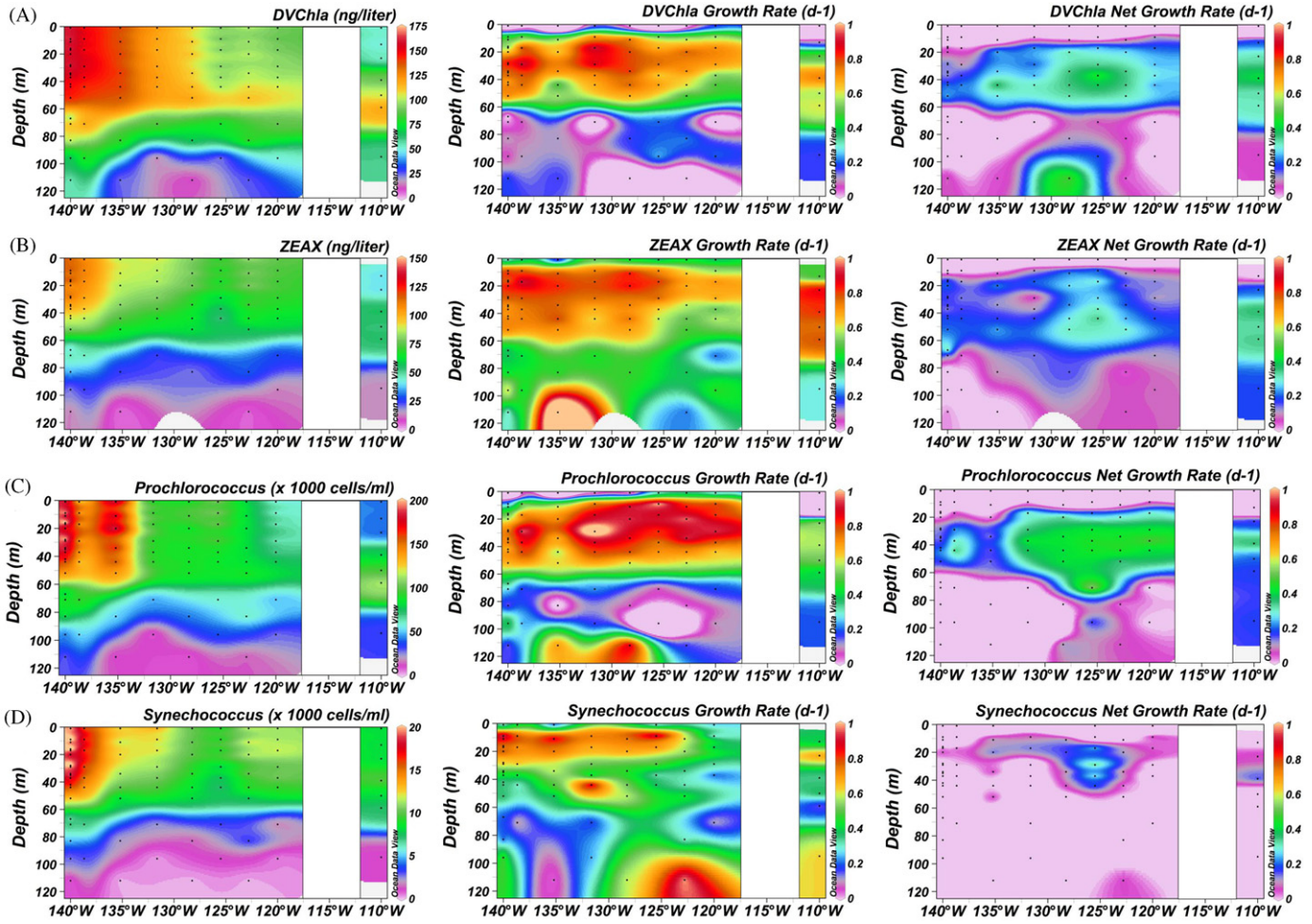

Fig. 8. Contour plots of the standing stocks and growth rates (μ and k) of prokaryotic pigments and cell abundances along the equatorial transect. Pigment-based stocks and rates were generated from HPLC data, whereas cell abundances and associated rates were generated from flow cytometry data. Three panels are shown for each parameter, with the left-most panel showing the standing stock, the middle panel showing the growth rates, and the right-most panel showing the net growth rates. From top to bottom, the panels are arranged as follows: (A) DVChl*a*, (B) ZEAX, (C) *Prochlorococcus*, (D) *Synechococcus*. Blank areas denote an absence of data.

Table 4
Pigment-based, taxon-specific estimates of phytoplankton growth (μ) and net growth (k) rates (d^{-1}). Shown are average rates for the depth-averaged euphotic zone ± 1 standard deviation from the mean. Averages for all data from both cruises are shown separately from averages of each cruise (EB04 and EB05). PER rates are not presented, as rate data were not available for much of the water column at many stations because of low peridinin concentrations. EB04, n=18; EB05, n=14.

	Both Cruises		EB04		EB05	
Pigment	μ	k	μ	k	μ	k
TChl*a*	0.53 ± 0.17	0.16 ± 0.11	0.54 ± 0.20	0.20 ± 0.09	0.51 ± 0.12	0.12 ± 0.12
MVChl*a*	0.57 ± 0.20	0.20 ± 0.11	0.58 ± 0.25	0.24 ± 0.10	0.56 ± 0.12	0.16 ± 0.11
DVChl*a*	0.34 ± 0.15	−0.01 ± 0.13	0.32 ± 0.16	0.00 ± 0.13	0.37 ± 0.13	−0.02 ± 0.14
ZEAX	0.54 ± 0.14	0.08 ± 0.10	0.49 ± 0.15	0.05 ± 0.09	0.60 ± ± 0.12	0.11 ± 0.12
FUCO	0.86 ± 0.32	0.33 ± 0.20	0.87 ± 0.42	0.40 ± 0.24	0.85 ± 0.12	0.24 ± 0.09
HEX	0.46 ± 0.23	0.24 ± 0.09	0.40 ± 0.28	0.24 ± 0.09	0.53 ± 0.09	0.25 ± 0.10
BUT	0.69 ± 0.10	0.29 ± 0.11	0.71 ± 0.09	0.33 ± 0.07	0.66 ± 0.09	0.24 ± 0.14

(0.20 ± 0.11 d^{-1}) were similar to the total, again with EB04 slightly exceeding EB05 rates (0.24 ± 0.10 d^{-1} *versus* 0.16 ± 0.11 d^{-1}). In contrast, and consistent with the results presented previously, DVChl*a* (*Prochlorococcus*) net rates were essentially zero for both cruises (−0.01 ± 0.13 d^{-1} overall, with EB04 = 0.00 ± 0.13 d^{-1} and EB05 = −0.02 ± 0.14 d^{-1}). FUCO, HEX and BUT net rates for both cruises ranged from 0.24-0.33 d^{-1}, higher than the overall community net rate of 0.16 d^{-1}. FUCO and BUT net rates were higher for EB04 relative to EB05, compared to little inter-cruise difference for HEX.

Because depth-averaged rate measurements and integrated standing stocks were similar among transects and cruises, only mean integrated rates of taxon-specific production and net production (production − consumption) rates are presented in Table 5. Production of TChl*a* on both cruises was 15.7 ± 5.5 μg m^{-2} d^{-1}, with 30% escaping microzooplankton grazing (net production = 4.7 ± 3.3 μg Chl *a* m^{-2} d^{-1}). Most of the net production was from eukaryotic groups, as indicated by MVChl*a*, FUCO, HEX and BUT, which all showed excess net production of at least 30%. In contrast, prokaryotes showed little (ZEAX, 15%) or no (DVChl*a*) net production.

Table 5
Taxon-specific depth-integrated rates of production (PROD) and net production (NET = production − consumption). Shown are average rates ± 1 standard deviation from the mean (μg pigment $m^{-2} d^{-1}$). Averages for all data from both cruises are shown separately from averages of each cruise (EB04 and EB05). Note that PER rates are not calculated, as rate data are not available for much of the water column at many stations. EB04, n = 18; EB05, n = 14.

Pigment	Both Cruises		EB04		EB05	
	PROD	NET	PROD	NET	PROD	NET
TChl*a*	15.68 ± 5.54	4.72 ± 3.28	16.18 ± 6.95	5.79 ± 2.70	15.04 ± 3.05	3.34 ± 3.54
MVChl*a*	10.81 ± 4.13	3.82 ± 2.06	10.75 ± 5.19	4.46 ± 1.88	10.88 ± 2.31	3.01 ± 2.07
DVChl*a*	3.57 ± 2.00	−0.01 ± 1.23	3.46 ± 2.26	0.10 ± 1.26	3.71 ± 1.66	−0.16 ± 1.23
ZEAX	3.34 ± 1.38	0.49 ± 0.66	2.94 ± 1.28	0.29 ± 0.48	3.85 ± 1.39	0.75 ± 0.78
FUCO	1.40 ± 0.74	0.54 ± 0.40	1.47 ± 0.96	0.68 ± 0.48	1.31 ± 0.32	0.36 ± 0.12
HEX	4.11 ± 1.99	2.16 ± 0.88	3.53 ± 2.42	2.05 ± 0.89	4.84 ± 0.86	2.31 ± 0.88
BUT	3.26 ± 0.64	1.35 ± 0.52	3.25 ± 0.71	1.49 ± 0.34	3.29 ± 0.54	1.18 ± 0.66

4. Discussion

4.1. Community composition

HEX was the most concentrated accessory pigment at all stations during our cruises, suggesting that prymnesiophytes (formerly haptophytes) were the dominant eukaryotic phytoplankton (but see Tangen and Björnland, 1981 for the presence of HEX in prymnesiophyte symbionts of dinoflagellates). The importance of the HEX accessory pigment has been previously documented for the eastern equatorial Pacific (e.g., Chavez et al., 1990; Bidigare and Ondrusek, 1996; Mackey et al., 1996, 2002). A companion paper based on microscopical analyses (Taylor et al., 2011) shows that prymnesiophytes were distributed similarly to HEX, and were mainly in the < 6-μm size fraction. Moon-van der Staay et al. (2000) also found that HEX was present in the portion of the community that passed a 3-μm filter.

The depth distribution of BUT, the second-most prominent accessory pigment, suggests that pelagophytes are better adapted to lower light conditions than most phytoplankton (deeper pigment maxima relative to MVChl*a* or HEX) or need higher nutrient conditions as would be found closer to the ferricline. The latter is especially implied by the spatial distribution of BUT, which increased along with Fe concentrations from 110 to 140°W along the equator.

FUCO was present throughout the equatorial region but at low concentrations, suggesting that diatom biomass was relatively low, a conclusion supported by microscopy (Taylor et al., 2011). In fact, our highest FUCO concentrations (~25 ng $liter^{-1}$) were lower than those reported by Bidigare and Ondrusek (1996), who found a subsurface (~80 m) maximum of > 45 ng $liter^{-1}$ FUCO at ~1°N, 140°W during the US JGOFS EqPac Survey II cruise. In contrast, other pigments were generally present at higher concentrations during the present cruises than EqPac Survey II. In addition, FUCO values were relatively invariant in depth profiles. The only exceptions were in areas of down sloping isopycnals at 2-4°N and 2-4°S, which suggests that diatoms were recently advected to these downwelling areas from the equator. FUCO concentration was also anomalously high in the surface at 0.5°N, 132°W while all other populations, except PER, were low. Fe concentration was high in this area immediately below the stratified upper 40 m, suggesting that the FUCO and PER were able to take advantage of the Fe gradient here more efficiently than other taxa, perhaps because higher Fe levels were present closer to the surface (and hence more light was available).

PER was detectable at low levels in all samples, while microscopy indicated that dinoflagellates averaged 45% of the depth-integrated autotrophic biomass (Taylor et al., 2011). Thus, the absence of PER in many dinoflagellate lineages can lead to a drastic underestimate of their importance in the open oceans from pigment indicators (e.g., Chesnick et al., 1997; Yoon et al., 2002). Nevertheless, the companion paper by Taylor et al. (2011) shows that the microscopy-based biomass distributions of the dinoflagellates were remarkably similar to the PER distributions – suggesting that even though PER was present at low levels, it is still reasonable to use as a proxy for dinoflagellate cell distributions. Dinoflagellates (PER) tended to co-occur where the biomass of other eukaryotic phytoplankton was high, but usually with a near-surface maximum. This result is consistent with Iriarte and Fryxell (1995), who found that dinoflagellates were concentrated near the surface, decreasing gradually with depth, during the EqPac cruises at 0°, 140°W. At stations where nutrients were lower, dinoflagellates displayed subsurface maxima near the nitracline.

Overall, stations with high pigment biomass were spatially partitioned, with PER usually highest at the surface, HEX also high at the surface but displaying more prominent subsurface maxima, BUT low at the surface with a deeper subsurface maxima than HEX, and FUCO relatively uniform and low throughout the euphotic zone (Fig. 4). Where nutrients were low, like at 110°W, all populations tended to have prominent subsurface maxima near the nitracline, but pelagophytes still had high pigment concentrations deeper than the other taxa.

4.2. Spatial patterns in phytoplankton distribution relative to Fe

During EB04, Fe surface concentrations increased ~6-fold along the equator from 110 to 140°W (< 0.1 to 0.6 nM, respectively). TChl*a* and DVChl*a* showed the same pattern of increasing concentration from east to west. These gradients are also reflected north and south of the equator, as revealed by the two meridional transects at 140°W (Sept. 2005) and 110°W (Dec. 2004). For instance, in the equatorial zone between the equator and 1.5°S along the 140°W transect, surface Fe and all phytoplankton pigments were high, whereas in the same latitudinal region along the meridional transect at 110°W, Fe and pigment concentrations were low in the surface waters north and south of the equator.

Along with the spatial patterns in Fe concentration, we observed that areas with high pigment concentrations in the upper 80 m coincided with one of the following conditions: 1) areas of upwelling of high Fe-containing water (e.g., the equatorial region at 140°W), 2) locations with high Fe in the surface layer, such as between 1.5°S and the equator at 140°W, or 3) areas with strong TIW activity (two stations along the 0.5°N transect).

In contrast, when undetectable levels of Fe were present at the surface waters or at depth in the EUC, surface biomass was low regardless of upwelling activity. For instance, despite apparent

upwelling at ~1°S, 110°W, undetectable levels of Fe were present at the top of the EUC (~70 m) and no surface pigment maximum was evident. At this station, and others where Fe was low, pronounced deep pigment maxima were found at the depth of the nutricline. For example, deep pigment maxima were found east of 0°, 130°W, where there was upwelling to the surface but low Fe at depth; at 0.5°N, 132°W, where Fe was high just below the stratified upper layer; and along the entire 110°W transect, where Fe was low and upwelling evident in places. Thus, pronounced subsurface maxima appear indicative of Fe-poor regions, whereas surface pigment maxima indicate Fe-sufficient regions. These patterns are consistent with the view that Fe limits biomass accumulation (Kolber et al., 1994; Martin et al., 1994; Coale et al., 1996a, b, 1998), and that phytoplankton have lower cellular pigment contents under Fe-limiting conditions in culture (Hardie et al., 1983; Greene et al., 1991; Geider et al., 1993; Wilhelm et al., 1996).

Since pigment:carbon biomass ratios are known to vary substantially with growth conditions, it is reasonable to question whether high pigment concentrations also represent high cellular carbon concentrations. On these cruises, where DVChl*a* was high at the surface, so was the cell abundance of *Prochlorococcus* (e.g., see Fig. 8). However, at depth, high DVChl*a* was not always reflected in high cell abundance. For instance, high DVChl*a* and cell abundance co-occurred only at 110°W on the equator (Fig. 8); to the west, deep DVChl*a* maxima were associated with low abundance *of Prochlorococcus*. Further, comparing pigments to microscopy-generated biomass distributions (data not shown, but see Taylor et al., 2011), reveals that high surface concentration of eukaryotic pigments tends to translate into high carbon biomass (i.e., high C:pigment ratios), whereas, high pigment content at depth reflects lower carbon biomass (low C:pigment). Indeed, as the companion paper by Taylor et al. (2011) shows, autotrophic carbon falls off sharply below the 10% light level, unlike the pattern seen for TChla at many stations where there are deep-chlorophyll maxima.

While we found near-surface pigment maxima in our sampling at the equator and 140°W, pronounced subsurface maxima were observed at 140°W, 2°S - 2°N during the JGOFS EqPac Survey II cruise (Bidigare and Ondrusek, 1996). The difference could be due to Fe concentrations. Surface Fe concentrations at 140°W during our cruises averaged 0.48 ± 0.14 nM (n=7), in contrast to surface Fe concentrations of <0.03 nM during the EqPac cruise (Coale et al., 1996a; Gordon et al., 1997). Thus, conditions during the Survey II cruise, while indicative of normal upwelling, supplied much lower Fe to the surface layer than during the EB cruises, leading to subsurface pigment maxima. Indeed, Bidigare and Ondrusek's (1996) pigment data at 140°W are quite similar to distributions observed on the EB04 cruise at 110°W, and with subsurface pigment maxima of approximately the same magnitudes. Fe concentrations at 110°W in 2004 were also quite similar to EqPac measurements both at the surface (~0.025 *versus* <0.03 nM, respectively) and at 100 m (~0.09 *versus* 0.1-0.35 nM). Kaupp et al. (2011) consider the possibility that Fe concentration in the EUC changes with variations in the amount of source material to the west. Such variability would be consistent with the pigment trends found here.

Contrary to expectation, phototrophic prokaryotes, as indicated by DVChl*a*, ZEAX and cell abundances of *Prochlorococcus* and *Synechococcus*, varied most in response to Fe-availability. Previous studies have shown that picoplankton populations can be physiologically stressed by low ambient Fe concentrations, despite their smaller size and presumed better fitness for low-Fe conditions (e.g., Greene et al., 1994; Henley and Yin, 1998, Barber and Hiscock, 2006). Nevertheless, our data suggest that *Prochlorococcus*, at least, is better able to cope with lower Fe conditions than other phytoplankton groups. For instance, on the 110°W transect from 2-4°S, a relatively stratified area with high Fe available at depth but no upwelling to surface waters, *Prochlorococcus* abundance and ZEAX concentrations were very high, whereas DVChl*a* and eukaryotic population indicator pigments showed subsurface maxima. The low *Synechococcus* abundances in surface water along with the DVChl*a* subsurface maxima suggest that this area was more oligotrophic (in terms of Fe) than other areas with high surface DVChl*a*.

In accordance with its photoprotective role, as well as typical cell distributions of *Prochlorococcus* and *Synechococcus*, ZEAX was usually high at the surface, decreasing with depth. The only stations where ZEAX was high at depth were on the equatorial transect at 110° and 116°W, co-occurring with abundant *Prochlorococcus* cells and DVChl*a* subsurface maxima (DVChl*a* was >45% higher at depth than in the surface, compared to 12-23% higher at other stations). These elevated ZEAX concentrations were presumably due to favorable conditions for *in situ* net accumulation of *Prochlorococcus*. At 140°W, 2.5°N, high ZEAX was found at 70 m along with all the other pigments except FUCO. Given the downward sloping isopycnals from the high biomass area in the equatorial region to 2.5°N, the elevated deep concentration of ZEAX at this location most likely reflected a surface assemblage that had been recently subducted.

4.3. Relationship between Fe and phytoplankton biomass

Upwelling of Fe from the EUC is considered the main source of Fe in the eastern equatorial Pacific (Wells et al., 1995; Coale et al. 1996a, Gordon et al., 1997, 1998; Kaupp et al., 2011). Thus, it seems reasonable to suppose that stations with a high supply rate of Fe from the EUC would show higher phytoplankton biomass. Consistent with this, a strong relationship is found between euphotic zone-integrated TChl*a* and Fe for equatorial stations with upwardly doming isopycnals (linear regression: TChl*a*=23.67+0.16(Fe), n=10, r^2=0.81, Fig. 9A). DVChl*a* also shows a significant positive relationship with Fe (DVChl*a*=7.44 + 0.12(Fe), n=10, r^2==0.62). FUCO, however, was relatively invariant and did not correlate with Fe (Fig. 9A). When all stations except for two at 0.5°N (described below) showing upwelling in the equatorial region (2°N-2°S) are included in the regression (n=18), the relationship is essentially the same, but the correlation coefficient is slightly lower (TChl*a*=23.94+0.15(Fe), r^2=0.75; DVChl*a*=7.29+0.11(Fe), r^2=0.57; Fig. 9B). In microscopical examination of the community, Taylor et al. (2011) also found higher heterotrophic and autotrophic biomass associated with upwelling and elevated Fe. In addition, increases in the >20-μm diatom biomass were associated with many of the upwelling areas, even though the smaller diatoms showed no obvious changes (Taylor et al., 2011).

Tropical instability waves (TIW) have been shown to enhance TChl*a* concentration in the equatorial Pacific, likely due to enhanced mixing and input of new Fe into surface waters (Foley et al., 1997; Strutton et al., 2001). The two upwelling stations along the 0.5°N transect that were excluded from the second regression described above were at stations strongly affected by a TIW (as suggested by the meridional component of the current velocity vector exceeding 35 cm sec^{-1} in the upper 70 m). These stations were characterized by very high pigment concentrations; however, Fe concentrations were very low in and directly below the euphotic zone (Fig. 9C). Although overall autotrophic biomass was not significantly higher at these stations, Taylor et al. (2011) did find proportionately higher biomass from >20-μm diatoms and autotrophic dinoflagellates, as well as in other areas with upwelling. This suggests that the larger size fractions of the

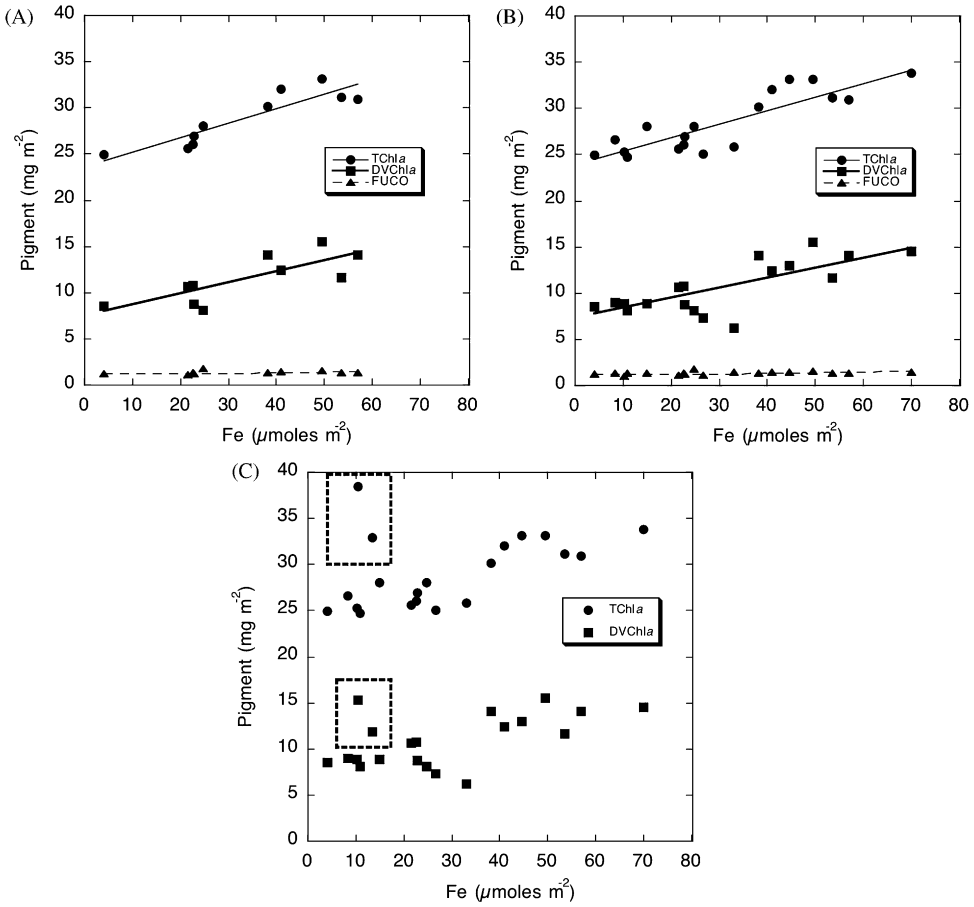

Fig. 9. Total Chlorophyll *a*, divinyl chlorophyll *a*, and fucoxanthin (mg m^{-2}) as a function of dissolved Fe (μmoles m^{-2}), all integrated over the depth of the euphotic zone. Panel A shows data only from upwelling stations along the equator; Panel B shows all upwelling stations occupied on both cruises, with the exception of two anomalous stations from the 0.5°N transect; Panel C shows all upwelling stations from both cruises, with data from the two anomalous stations from the 0.5°N transect included (boxed). Linear regression data for Panel A: Total Chlorophyll *a*=23.67+0.15(Fe), r^2=0.84, Divinyl Chlorophyll *a*=7.44+0.12(Fe), r^2=0.62, Fucoxanthin=1.25+0.00(Fe), r^2=0.10. Panel B: Total Chlorophyll *a*=23.94+0.15 (Fe), r^2=0.75, Divinyl Chlorophyll *a*=7.29+0.11(Fe), r^2=0.57, Fucoxanthin=1.22+0.00(Fe), r^2=0.17.

phytoplankton community were stimulated by Fe availability in the past, if we assume that larger size classes of phytoplankton indicate more nutrient availability in surface waters. Further, mean heterotrophic micrograzer (20-200 μM) biomass was double in this area, relative to the means of other transects (Taylor et al., 2011). Décima et al. (2011) found high mesozooplankton biomass in this area, strongly dominated by the smaller size classes (0.2-2 mm), along with the highest grazing estimates of the EB05 zonal transect. These data suggest a community that had largely incorporated a pulse in surface-layer Fe input into larger autotrophs, which then stimulated the grazing community. The time scale of this uptake event may have been as little as 2 to 3 days earlier, if we can use the results of the IronEx II *in situ* experiment as a guide (Coale et al., 1996b). In that experiment, within 2 to 3 days of the initial Fe fertilization, surface Fe was greatly depleted, whereas pigment concentrations (including FUCO) increased, along with micro- and meso-zooplankton community abundances (Coale et al., 1996b, Landry et al., 2000, Rollwagen-Bollens and Landry, 2000). Alternatively, the high pigment concentrations seen here in the TIW affected area may have been advected to 0.5°N by the TIW, with the waters originally being seeded with Fe at the equator; again, this could have occurred in as little as 2-3 days, given the rates of water movement in the equatorial divergence zone (Landry et al., 1997). Indeed, Roman et al. (2002) speculated that higher mesozooplankton biomass found poleward of the equator during EqPac was due to a time-delay in grazer response to phytoplankton growth.

These data support the hypothesis that variations in the natural availability of Fe affect phytoplankton biomass, as has also been shown by the system response to mesoscale Fe enrichment (e.g., Coale et al., 1996b). However, direct experimental addition of Fe to equatorial surface waters has been shown to depress *Prochlorococcus* biomass (Landry et al., 2000), while our results show a positive relationship between Fe and *Prochlorococcus*. This unexpected result suggests that Fe supplied from upwelling affects the system differently from Fe added in high concentration to surface waters, perhaps because of light availability. It appears that at low light, such as the base of the euphotic zone, small (high surface area:volume) photosynthetic prokaryotes are favored over diatoms, whereas in the surface ocean, high light levels allow diatoms to accumulate more biomass by escaping predation, i.e., their net growth is higher, with the addition of new Fe. Thus, the community in this HNLC region is analogous to those in oligotrophic oceanic regions, where the phytoplankton community is also dominated by prokaryotic autotrophs. In the latter case, however, the limiting nutrient is nitrate, and this limiting nutrient is also principally delivered at the base of the euphotic zone. Further, atmospheric deposition of Fe in the surface well-lit layer (analogous to the addition of Fe to experimental incubation bottles under constant light) would act as "new Fe". Although this may only represent ~2-10% of the daily input of new Fe to the system (Coale et al., 1996a; Gordon et al., 1997; Kaupp et al., 2011), integrating this surface deposition over several days may contribute significantly to diatom growth. Likewise, enhanced

Fe availability from photo-oxidation of remineralized Fe (Barbeau et al., 2001) in upwelled waters diverging polewards from the equator may also allow for preferential growth of surface diatom populations.

4.4. Phytoplankton growth rates

Past investigations of phytoplankton growth and microzooplankton grazing in the equatorial Pacific have focused principally on the mixed layer or deep chlorophyll maximum, with often only a few stations or dilution experiments reported per study (Landry et al., 1995a, b, 2003; Verity et al., 1996; Latasa et al., 1997). Here, we have used a reduced 2-treatment approach to generate a rate profile at 8 depths per station, for 32 stations and two cruises (256 experiments). Thus, we can examine in detail, at the vertical and horizontal spatial scales of variability, process rates for co-occurring dominant phytoplankton groups. A linear relationship between dilution level and net growth rate is assumed in our analysis, and also expected from the results of numerous experiments performed previously in the equatorial Pacific (e.g., Landry et al., 1995b). In addition, over the course of this study, we confirmed the linear model of net growth response to dilution by conducting a limited number of comparative experiments using the traditional dilution array (results reported in Landry et al., in press) with replicated treatments at each of 5 dilution levels. Another refinement of the present study is the complementary use of microscopical, flow cytometric and HPLC pigment analyses to quantify pigment:biomass ratios so that biomass growth rate assessments would not be confounded by changes in cellular pigment content over the course of our incubations.

Depth-averaged growth rates for the phytoplankton community were 0.53 d^{-1}, with 70% of daily production consumed by micrograzers. Growth rates were highest on average for diatoms and pelagophytes (0.86 and 0.69 d^{-1}, respectively), whereas prymnesiophytes (0.46 d^{-1}) grew at a rate slightly lower than the community average. The relative trends of these growth rates are similar to those from EqPac experiments (Verity et al., 1996; Latasa et al., 1997). The euphotic zone average growth rate of diatoms (0.86 d^{-1}) understates their much higher rates measured in the surface layer (1.60 d^{-1}; surface to 13% light level). Thus, while representing only a small percentage of the total pigment and carbon biomass in the equatorial Pacific (and presumably also having the most limited production as a group by iron availability), diatoms contribute disproportionately to community production and the net growth that escapes microherbivore consumption. Micrograzers nonetheless consume a substantial amount (60%) of diatom production in the equatorial Pacific, and their mode of feeding on and egesting individual cells is likely responsible for the high proportion of detrital biogenic silica and rapid Si remineralization found in this region (Krause et al., 2011).

The depth-averaged growth rate for Prochlorococcus (0.34 d^{-1}) was slower than for all of the major groups of eukaryotic phytoplankton, and all of the daily production was consumed by micrograzers. This mean rate is about half of the approximately one doubling per day rate commonly reported for Prochlorococcus in the equatorial Pacific (e.g., Landry et al., 1995b, 2003; Vaulot et al., 1995; Binder et al., 1996; Liu et al., 1999), from experiments which reflect mainly the rates at higher light levels of the upper euphotic zone. However, our mixed-layer estimates (0.59 ± 0.23 d^{-1}) are essentially the same as previous studies.

In contrast to what one might expect intuitively, we found no significant relationship between phytoplankton growth rates and Fe concentration in our experiments. The explanation for this comes from the nutrient-limited chemostat analogy that has been used to describe the HNLC equatorial Pacific (Frost and Franzen, 1992). According to chemostat theory, the amount of limiting Fe in the feed supply (upwelling from the EUC) should act mainly to regulate the biomass level in the system. Growth rate at steady state, however, is regulated by the dilution rate, in this case the removal rate due to grazing mortality. Consistent with theory, the biomass (pigment and biovolume) of cultured phytoplankton has been shown to decrease in response to Fe-deficiency, even as Fe uptake rates normalized to the cell surface area remain constant, allowing the smaller cells to maintain a high rate of growth at low levels of Fe availability (e.g., Sunda and Huntsman, 1995). Like a chemostat, our data suggest that stock levels of phytoplankton were controlled by Fe supply and that Fe was generally sufficient to allow for rapid phytoplankton growth. Further, our data show that the grazing mortality rates of microzooplankton feeding on phototrophic bacteria essentially matched the growth rates of the cells – like a chemostat at steady state. These tightly coupled growth and mortality rates lead to rapid remineralization of Fe (e.g., Hutchins et al., 1993; Barbeau et al., 1996; Twining and Fisher, 2004), and thereby contribute to sustaining high growth. For eukaryotic phytoplankton, a comparable match of grazing mortality to growth is provided by the combination of micro- and mesozooplankton consumers (Décima et al., 2011; Landry et al., 2011). Thus, a tight coupling between growth, grazing and recycled Fe is believed to prevail for the community as a whole.

The relative constancy of growth rates several degrees away from the equatorial divergence implies that the community is insulated in some way from a gradual depletion of bioavailable Fe due to export losses as waters are advected to the north and south. The magnitude of daily euphotic zone loss of Fe can be approximated in relation to carbon export, which Th-based estimates during the US JGOFS EqPac Program set at 2-5 mmole C m^{-2} d^{-1} (Buesseler et al., 1995). If Fe is exported at the 10^5 molar C:Fe ratio as its composition in phytoplankton (Sunda and Huntsman, 1995), then Fe should be lost at a rate of 20-50 nmol Fe m^{-2} d^{-1}. However, if Fe recycling is two or three times more efficient than C (e.g., Hutchins et al., 1993; Barbeau et al., 1996, Twining and Fisher, 2004), its daily export loss could be as low as 7-18 nmol Fe m^{-2} d^{-1}. Several mechanisms may replenish export losses of this magnitude with a slow trickle of Fe to surface waters. For example, while Coale et al. (1996a) and Kaupp et al. (2011) have estimated that atmospheric deposition of Fe is at least 10× lower than Fe delivery from upwelling at the equator, their mean atmospheric estimates of 5-25 nmole Fe m^{-2} d^{-1} are similar in magnitude to export losses. Another source of bio-available Fe in upwelled equatorial surface waters would be the gradual photo-oxidative release of complexed Fe that likely occurs in the surface mixed layer during advective transport (e.g., Johnson et al. 1994). Grazing processes at and away from the equator may also lock some of the previously grazed Fe into slower release mechanisms, as envisioned in Frost and Franzen's (1992) chemostat model. "Dissolved" Fe, for instance, includes colloidal and siderophore-complexed Fe (Gledhill and van den Berg, 1994; Rue and Bruland, 1995; van den Berg, 1995; Witter and Luther, 1998; Powell and Donat, 2001; Wu et al., 2001; Berquist et al., 2007), with Fe binding differences that affect availability to prokaryotic versus eukaryotic phytoplankton (Hutchins et al., 1999; Boye and van den Berg, 2000; Nishioka and Takeda, 2000; Nodwell and Price, 2001).

In addition to grazing controls of phytoplankton growth, our results suggest that one must consider how the low light levels, where newly upwelled Fe enters the base of the euphotic zone from the EUC, affects the uptake and distribution of Fe among competing types and size classes of phytoplankton. As discussed

above, this main route of new Fe delivery to equatorial waters seems to be more favorable for development of a small-size dominated community than if the new Fe were pulsed directly into surface waters. Once the level of standing stock is established by the inventory of available Fe, however, microzooplankton grazing is a key factor in regulating the densities of small cells, and in sustaining high growth rates by remineralization of Fe. Thus, by the time the stimulatory upwelling effect is mixed into shallower depths with abundant light, the community is already tightly coupled and recycling dependent, such that biomass gains of individual functional groups of phytoplankton can only be made slowly at the expense of the others.

5. Conclusions

The present study is the first to compare stocks and rates for dominant phytoplankton groups over an extensive geographical area of the eastern equatorial Pacific, and it is the first to resolve taxon-specific growth rates in depth profiles through the shallow and deep euphotic zone. From the analysis of 256 rate estimates for each taxonomically defined group, we found no significant spatial or temporal pattern in phytoplankton growth rates. However, diatom growth rates were significantly higher than those of any other group. In contrast, spatial patterns of phytoplankton pigments, as well as the abundances of the picoplankton *Prochlorococcus* and *Synechoccocus*, did suggest a relationship with Fe concentration. Most significantly, euphotic zone integrated TChl*a* was positively correlated ($r^2=0.81$) with integrated Fe at equatorial upwelling stations, showing that increasing Fe inventories co-occur with increasing phytoplankton biomass. This response was mostly attributable to changes in *Prochlorococcus* (as DVChl*a*), with neither FUCO nor other eukaryotic-specific pigments showing significant trends with dissolved Fe concentration. Further, areas with lower Fe availability were associated with pronounced subsurface pigment maxima, whereas areas with higher Fe had slight subsurface maxima with high biomass extending to the surface. These data suggest that natural variability in Fe concentration directly determines standing stock of the total phytoplankton community, but not growth rates.

Previous research in the equatorial Pacific has pointed to increased availability of Fe leading to a disproportionate increase of larger phytoplankton, particularly diatoms, whereas picoplankton biomass stayed relatively constant, controlled by microzooplankton grazing. In contrast, the current results show that picoplankton biomass increases along with general community biomass, and that diatom biomass does not become disproportionately higher, despite the fact that considerable diatom (and other eukaryote) production escapes microzooplankton grazing control. These data suggest that Fe introduced into the base of the euphotic zone, as occurs with Fe supplied from the EUC through upwelling, appears to have a different effect on community structure than Fe added to surface waters or well-lit incubation bottles (as from atmospheric deposition, Fe-fertilization projects, or deck-board Fe-amended incubation experiments). Under high light, diatoms grow at substantially higher rates than the rest of the community. In contrast, when Fe is supplied from the base of the euphotic zone, where low light levels do not favor the explosive growth of large phytoplankton, the entire community responds to the addition of Fe, evolving together. By the time the upwelled water has reached the high light surface ocean where larger cells would be favored if the nutrient levels were sufficient, the limiting nutrient levels are much lower and the community is effectively constrained by the tight coupling of grazing, growth and recycling. This requirement for higher light along with Fe also explains why TIW activity often results in increased production and disproportionate growth of diatoms over other groups – the rapid mixing of nutrient-rich deep water into well-lit surface waters favors diatoms over other groups.

Acknowledgments

We thank the Captain and crew of the R/V *Roger Revelle* for their professional and enthusiastic support of this project. Gene Pillard, the Resident Technician from SIO, was indispensable to the success of this field project. Dr. Jules Hummon (Department of Oceanography, University of Hawaii at Manoa) is also thanked for reducing the ADCP data so that mere mortals could interpret it. We would also like to thank our collaborators in the Dugdale-Wilkerson group, especially Vicky Hogue and Al Marchi, for the use of their macronutrient data. This work was funded by subcontracts to Scripps Institution of Oceanography and the University of Hawaii at Manoa from NSF Biocomplexity grant OCE 03-22074, administered through Oregon State University (Dr. D. Nelson, PI). This is SOEST contribution 7678.

References

Andersen, R.A., Saunders, G.W., Paskind, M.P., Sexton, J.P., 1993. The ultrastructure and 18S rRNA gene sequence for *Pelagomonas calceolata* gen. et sp. nov., and the description of a new algal class, the Pelagophyceae classis nov. Journal of Phycology 29, 701–716.

Arpin, N., Svec, W.A., Liaaen-Jensen, S., 1976. New fucoxanthin-related carotenoids from *Coccolithus huxleyi*. Phytochemistry 15, 529–532.

Barbeau, K., Moffett, J.W., Caron, D.A., Croot, P.L., Erdner, D.L., 1996. Role of protozoan grazing in relieving iron limitation of phytoplankton. Nature 380, 61–64.

Barbeau, K., Rue, E.L., Bruland, K.W., Butler, A., 2001. Photochemical cycling of iron in the surface ocean mediated by microbial iron(III)-binding ligands. Nature 413, 409–413.

Barber, R.T., Sanderson, M.P., Lindley, S.T., Chai, F., Newton, J., Trees, C.C., Foley, D.G., Chavez, F.P., 1996a. Regulation of primary productivity rate in the equatorial Pacific. Limnology and Oceanography 36, 1803–1815.

Barber, R.T., Sanderson, M.P., Lindley, S.T., Chai, F., Newton, J., Trees, C.C., Foley, D.G., Chavez, F.P., 1996b. Primary productivity and its regulation in the equatorial Pacific during and following the 1991-1992 El Niño. Deep-Sea Research II 43, 933–969.

Barber, R.T., Hiscock, M.R., 2006. A rising tide lifts all phytoplankton: growth response of other phytoplankton taxa in diatom-dominated blooms. Global Biogeochemical Cycles 20 (GB4S03. doi:10.1029/2006GB002726.

Berquist, B.A., Wu, J., Boyle, E.A., 2007. Variability in oceanic dissolved iron is dominated by the colloidal fraction. Geochimica et Cosmochimica Acta 71, 2960–2974.

Bidigare, R.R., Van Heukelem, L., Trees, C.C., 2005. Analysis of algal pigments by high-performance liquid chromatography. In: Andersen, R.A. (Ed.), Algal Culturing Techniques. Academic Press, New York, NY, pp. 327–345.

Bidigare, R.R., Ondrusek, M.E., 1996. Spatial and temporal variability of phytoplankton pigment distributions in the central equatorial Pacific Ocean. Deep-Sea Research II 43, 809–833.

Binder, B.J., Chisholm, S.W., Olson, R.J., Frankel, S.L., Worden, A.Z., 1996. Dynamics of picophytoplankton, ultraphytoplankton and bacteria in the central equatorial Pacific. Deep-Sea Research II 43, 907–931.

BjØrnland, T., Liaaen-Jensen, S., 1989. Distribution patterns of carotenoids in relation to chromophyte phylogeny and systematics. In: Green, J.C., Leadbeater, B.S.C., Diver, W.L. (Eds.), The Chromophyte Algae: Problems and Perspectives. Clarendon Press, Oxford, pp. 37–61.

Boye, M., van den Berg, C.M.G., 2000. Iron availability and the release of iron-complexing ligands by *Emiliana huxleyi*. Marine Chemistry 70, 277–287.

Brown, S.L., Landry, M.R., Selph, K.E., Yang, E.J., Rii, Y.M., Bidigare, R.R., 2008. Diatoms in the desert: Phytoplankton community response to a mesoscale eddy in the subtropical North Pacific. Deep-Sea Research II 55, 1321–1333.

Buesseler, K.O., Andrews, J.A., Hartman, M.C., Belastock, R., Chai, F., 1995. Regional estimates of the export flux of particulate organic carbon derived from thorium-234 during the JGOFS EqPac program. Deep-Sea Research II 42, 777–804.

Buma, A.G.J., Bano, N., Veldhuis, M.J.W., Kraay, G.W., 1991. Comparison of pigmentation of two strains of prymnesiophyte *Phaeocystis* sp. Netherlands Journal of Sea Research 27, 173–182.

Campbell, L., Vaulot, D., 1993. Photosynthetic picoplankton community structure in the subtropical North Pacific Ocean near Hawaii (station ALOHA). Deep-Sea Research I 40, 2043–2060.

Chavez, F.P., Buck, K.R., Barber, R.T., 1990. Phytoplankton taxa in relation to primary production in the equatorial Pacific. Deep-Sea Research 37, 1733–1752.

Chavez, F.P., Buck, K.R., Coale, K.H., Martin, J.H., DiTullio, G.R., Welschmeyer, N.A., Jacobson, A.C., Barber, R.T., 1991. Growth rates, grazing, sinking and iron limitation of equatorial Pacific phytoplankton. Limnology and Oceanography 36, 1816–1833.

Chesnick, J.M., Kooistra, W.H.C.F., Wellbrock, U., Medlin, L.K., 1997. Ribosomal RNA analysis indicates a benthic pennate diatom ancestry for the endosymbionts of the dinoflagellates *Peridinium foliaceum* and *Peridinium balticum* (Pyrrhophyta). Journal of Eukaryotic Microbiology 44, 314–320.

Coale, K.H., Fitzwater, S.E., Gordon, R.M., Johnson, K.S., Barber, R.T., 1996a. Control of community growth and export production by upwelled iron in the equatorial Pacific Ocean. Nature 379, 621–624.

Coale, K.H., Johnson, K.S., Fitzwater, S.E., Gordon, R.M., Tanner, S., Chavez, F.P., Ferioli, L., Sakamoto, C., Rogers, P., Millero, F., Steinberg, P., Nightingale, P., Cooper, D., Cochlan, W.P., Landry, M.R., Constantinou, J., Rollwagen, G., Trasvinastar, A., Kudela, R., 1996b. A massive phytoplankton bloom induced by an ecosystem-scale iron fertilization experiment in the equatorial Pacific Ocean. Nature 383, 495–501.

Coale, K.H., Johnson, K.S., Fitzwater, S.E., Blain, S.P.G., Stanton, T.P., Coley, T.L., 1998. IronEx-I, an *in situ* iron-enrichment experiment: Experimental design, implementation and results. Deep-Sea Research II 45, 919–945.

Décima, M., Landry, M.R., Rykaczewski, R., 2011. Broad-scale patterns in mesozooplankton biomass and grazing in the Eastern Equatorial Pacific. Deep-Sea Research II 58 (3–4), 387–399.

Dugdale, R.C., Wilkerson, F.P., Chai, F., Feely, R., 2007. Size-fractionated nitrogen uptake measurements in the equatorial Pacific and confirmation of the low Si-high-nitrate-low-chlorophyll condition. Global Biogeochemical Cycles 21 (GB2005. doi:10.1029/2006GB002722.

Dugdale, R.C., Chai, F., Feely, R.A., Measures, C.I., Parker, A.E., Wilkerson, F.P., 2011. The regulation of equatorial Pacific new production and pCO_2 by silicate-limited diatoms. Deep-Sea Research II 58 (3–4), 477–492.

Eppley, R.W., 1972. Temperature and phytoplankton growth in the sea. Fishery Bulletin 70, 1063–1085.

Feely, R.A., Boutin, J., Cosca, C.E., Dandonnneau, Y., Etcheto, J., Inoue, H.Y., Ishii, M., Le Quere, C., Mackey, D.J., McPhaden, M., Metzl, N., Poisson, A., Wanninkhof, R., 2002. Seasonal and interannual variability of CO_2 in the equatorial Pacific. Deep-Sea Research II 49, 2443–2469.

Foley, D.G., Dickey, T.D., McPhaden, M.J., Bidigare, R.R., Lewis, M.R., Barber, R.T., Lindley, S.T., Garside, C., Manov, D.V., McNeil, J.D., 1997. Longwaves and primary productivity variations in the equatorial Pacific at 0°, 140°W. Deep-Sea Research II 44, 1801–1826.

Frost, B.W., Franzen, N.C., 1992. Grazing and iron limitation in the control of phytoplankton stock and nutrient concentration: a chemostat analogue of the Pacific equatorial upwelling zone. Marine Ecology Progress Series 83, 291–303.

Garrison, D.L., Gowing, M.M., Huges, M.P., Campbell, L., Caron, D.A., Dennett, M.R., Shalapyonok, A., Olson, R.J., Landry, M.R., Brown, S.L., Liu, H.-B., Azam, F., Steward, G.F., Ducklow, H.W., Smith, D.C., 2000. Microbial food web structure in the Arabian Sea: A US JGOFS study. Deep-Sea Research II 47, 1387–1422.

Geider, R.J., Roche, J., Greene, R.M., Olaizola, M., 1993. Response of the photosynthetic apparatus of *Phaeodactylum tricornutum* (Bacillariophyceae) to nitrate, phosphate, or iron starvation. Journal of Phycology 29 (6), 755–766.

Gieskes, W.W.C., Kraay, G.W., 1986. Analysis of phytoplankton pigments by HPLC before, during and after mass occurrence of the microflagellate *Corymbellus aureus* during the spring bloom in the open northern North Sea in 1983. Marine Biology 92, 45–52.

Gledhill, M., van den Berg, C.M.G., 1994. Determination of complexation of iron(III) with natural organic complexing ligands in seawater using cathodic stripping voltammetry. Marine Chemistry 47, 41–54.

Gordon, R.M., Coale, K.H., Johnson, K.S., 1997. Iron distribution in the equatorial Pacific: Implications for new production. Limnology and Oceanography 42, 419–431.

Gordon, R.M., Johnson, K.S., Coale, K.H., 1998. The behaviour of iron and other trace elements during the IronEx-I and PlumEx experiments in the Equatorial Pacific. Deep-Sea Research II 45, 995–1041.

Greene, R.M., Geider, R.J., Falkowski, P.G., 1991. Effect of iron limitation on photosynthesis in a marine diatom. Limnology and Oceanography 36 (8), 1772–1782.

Greene, R.M., Kolber, Z.S., Swift, D.G., Tindale, N.W., Falkowski, P.G., 1994. Physiological limitation of phytoplankton photosynthesis in the eastern equatorial Pacific determined from variability in the quantum yield of fluorescence. Limnology and Oceanography 39 (5), 1061–1074.

Hardie, L.P., Balkwill, D.L., Stevens Jr., S.E., 1983. Effects of iron starvation on the physiology of the cyanobacterium *Agmenellum quadruplicatum*. Applied and Environmental Microbiology 45, 999–1006.

Henley, Y.J., Yin, Y., 1998. Growth and photosynthesis of marine *Synechococcus* (Cyanophyceae) under iron stress. Journal of Phycology 34, 94–103.

Hutchins, D.A., DiTullio, G.R., Bruland, K.W., 1993. Iron and regenerated production: evidence for biological iron recycling in two marine environments. Limnology and Oceanography 38, 1242–1255.

Hutchins, D.A., Witter, A.E., Butler, A., Luther III, G.W., 1999. Competition among marine phytoplankton for different chelated iron species. Nature 400, 858–861.

Iriarte, J.L., Fryxell, G.A., 1995. Micro-phytoplankton at the equatorial Pacific (140°W) during the JGOFS EqPac time series studies: March to April and October 1992. Deep-Sea Research II 42, 559–583.

Jeffrey, S.W., Vesk, M., 1997. Introduction to marine phytoplankton and their pigment signatures. In: Jeffrey, S.W., Mantoura, R.C.F., Wright, S.W. (Eds.), Phytoplankton pigments in oceanography: guidelines to modern methods. UNESCO Publ., Paris, pp. 37–82.

Johnson, K.S., Coale, K.H., Elrod, V.A., Tindale, N.W., 1994. Iron photochemistry in seawater from the equatorial Pacific. Marine Chemistry 46, 319–334.

Kaupp, L.J., Measures, C.I., Selph, K.E., Mackenzie, F.T., 2011. The distribution of dissolved Fe and Al in the upper waters of the eastern equatorial Pacific. Deep-Sea Research II 58 (3–4), 296–310.

Kolber, Z.S., Barber, R.T., Coale, K.H., Fitzwater, S.E., Greene, R.M., Johnson, K.S., Lindley, S., Falkowski, P.G., 1994. Iron limitation of phytoplankton photosynthesis in the equatorial Pacific Ocean. Nature 371, 145–149.

Krause, J.W., Nelson, D.M., Brzezinski, M.A., 2011. Biogenic silica production and the diatom contribution to primary production and nitrate uptake in the eastern equatorial Pacific Ocean. Deep-Sea Research II 58 (3–4), 434–448.

Landry, M.R., Hassett, R.P., 1982. Estimating the grazing impact of marine micro-zooplankton. Marine Biology 67, 283–288.

Landry, M.R., Haas, L.W., Fagerness, V.L., 1984. Dynamics of microplankton communities: experiments in Kaneohe Bay, Hawaii. Marine Ecology Progress Series 16, 127–133.

Landry, M.R., Constantinou, J., Kirshtein, J., 1995a. Microzooplankton grazing in the central equatorial Pacific during February and August, 1992. Deep-Sea Research II 42, 657–671.

Landry, M.R., Kirshtein, J., Constantinou, J., 1995b. A refined FLB-dilution approach for measuring the community grazing impact of microzooplankton, with experimental tests in the equatorial Pacific. Marine Ecology Progress Series 120, 53–63.

Landry, M.R., Barber, R.T., Bidigare, R.R., Chai, F., Coale, K.H., Dam, H.G., Lewis, M.R., Lindley, S.T., McCarthy, J.J., Roman, M.R., Stoecker, D.K., Verity, P.G., White, J.R., 1997. Iron and grazing constraints on primary production in the central equatorial Pacific: An EqPac synthesis. Limnology and Oceanography 42 (3), 405–418.

Landry, M.R., Ondrusek, M.E., Tanner, S.J., Brown, S.L., Constantinou, J., Bidigare, R.R., Coale, K.H., Fitzwater, S., 2000. Biological response to iron fertilization in the eastern equatorial Pacific (IronExII). I. Microplankton community abundances and biomass. Marine Ecology Progress Series 201, 27–42.

Landry, M.R., Kirchman, D.L., 2002. Microbial community structure and variability in the tropical Pacific. Deep-Sea Research II 49, 2669–2693.

Landry, M.R., Brown, S.L., Neveux, J., Dupouy, C., Blanchot, J., Christensen, S., Bidigare, R.R., 2003. Phytoplankton growth and microzooplankton grazing in HNLC waters of the equatorial Pacific: Community and taxon-specific rate assessments from pigment and flow cytometric analyses. Journal of Geophysical Research 108 (C12), 8142. doi:10.1029/2000JC000744.

Landry, M.L., Brown, S.L., Rii, Y.M., Selph, K.E., Bidigare, R.R., Yang, E.J., Simmons, M.P., 2008. Depth-stratified phytoplankton dynamics in Cyclone *Opal*, a subtropical mesoscale eddy. Deep-Sea Research II 55, 1348–1359.

Landry, M.R., Selph, K.E., Taylor, A.G., Décima, M., Balch, W.M., Bidigare, R.R., 2011. Phytoplankton growth, grazing and production balances in the HNLC equatorial Pacific. Deep-Sea Research II 58 (3–4), 524–535.

Landry, M.R., Selph, K.E., Yang, E.J., in press. Decoupled phytoplankton growth and microzooplankton grazing in the deep euphotic zone of the HNLC equatorial Pacific. Marine Ecology Progress Series.

Latasa, M., Landry, M.R., Schluter, L., Bidigare, R.R., 1997. Pigment-specific growth and grazing rates of phytoplankton in the central equatorial Pacific. Limnology and Oceanography 42, 289–298.

Levitus, S., Conkright, M.E., Reid, J.L., Najjar, R.G., Mantyla, A., 1993. Distribution of nitrate, phosphate and silicate in the world oceans. Progress in Oceanography 31, 245–273.

Liu, H., Landry, M.R., Vaulot, D., Campbell, L., 1999. *Prochlorococcus* growth rates in the central equatorial Pacific: an application of the f_{max} approach. Journal of Geophysical Research 104 (C2), 3391–3399.

Mackey, M.D., Mackey, D.J., Higgins, H.W., Wright, S.W., 1996. CHEMTAX – a program for estimating class abundances from chemical markers: Application to HPLC measurements of phytoplankton. Marine Ecology Progress Series 144, 265–283.

Mackey, D.J., Blanchot, J., Higgins, H.W., Neveux, J., 2002. Phytoplankton abundances and community structure in the equatorial Pacific. Deep-Sea Research II 49, 2561–2582.

Martin, J.H., Coale, K.H., Johnson, K.S., Fitzwater, S.E., Gordon, R.M., Tanner, S.J., Hunter, C.N., Elrod, V.A., Nowicki, J.L., Coley, T.L., Barber, R.T., Lindley, S., Watson, A.J., Van Scoy, K., Law, C.S., Liddicoat, M.I., Ling, R., Stanton, T., Stoeckel, J., Collins, C., Anderson, A., Bidigare, R., Ondrusek, M., Latasa, M., Millero, F.J., Lee, K., Yao, W., Zhang, J.Z., Friederich, G., Sakamoto, C., Chavez, F., Buck, K., Kolber, Z., Greene, R., Falkowski, P., Chisholm, S.W., Hoge, F., Swift, R., Yungel, J., Turner, S., Nightingale, P., Hatton, A., Liss, P., Tindale, N.W., 1994. Testing the iron hypothesis in ecosystems of the Equatorial Pacific Ocean. Nature 371, 123–129.

Measures, C.I., Yuan, J., Resing, J.A., 1995. Determination of iron in seawater by flow injection analysis using in-line preconcentration and spectrophotometric detection. Marine Chemistry 50, 3–12.

Measures, C.I., Landing, W.M., Brown, M.T., Buck, C.S., 2008. A commercially available rosette system for trace metal-clean sampling. Limnology and Oceanography-Methods 6, 384–394.

Menden-Deuer, S., Lessard, E.J., 2000. Carbon to volume relationships for dinoflagellates, diatoms, and other protist plankton. Limnology and Oceanography 45, 569–679.
Millie, D.F., Paerl, H.W., Hurley, J.P., 1993. Microalgal pigment assessments using high-performance liquid chromatography: A synopsis of organismal and ecological applications. Canadian Journal of Fisheries and Aquatic Sciences 50 (11), 2513–2527.
Minas, H.J., Minas, M., Packard, T.T., 1986. Productivity in upwelling areas deduced from hydrographic and chemical fields. Limnology and Oceanography 31, 1182–1206.
Moon-van der Staay, S.Y., van der Staay, G.W.M., Guillou, L., Vaulot, D., 2000. Abundance and diversity of prymnesiophytes in the picoplankton community from the equatorial Pacific Ocean inferred from 18S rDNA sequences. Limnology and Oceanography 45 (1), 98–109.
Monger, B.C., Landry, M.R., 1993. Flow cytometric analysis of marine bacteria with Hoechst 33342. Applied and Environmental Microbiology 59, 905–911.
Murray, J.W., Barber, R.T., Roman, M.R., Bacon, M.P., Feely, R.A., 1994. Physical and biological controls on carbon cycling in the equatorial Pacific. Science 266, 58–65.
Nishioka, J., Takeda, S., 2000. Change in the concentration of iron in different size fractions during growth of the oceanic diatom *Chaetoceros* sp.: importance of small colloidal iron. Marine Biology 137, 231–238.
Nodwell, L.M., Price, N.M., 2001. Direct use of inorganic colloidal iron by marine mixotrophic phytoplankton. Limnology and Oceanography 46 (4), 765–777.
Powell, R.T., Donat, J.R., 2001. Organic complexation and speciation of iron in the South and Equatorial Atlantic. Deep-Sea Research II 48, 2877–2893.
Roman, M.R., Dam, H.G., Le Borgne, R., Zhang, X., 2002. Latitudinal comparisons of equatorial Pacific zooplankton. Deep-Sea Research II 49, 2695–2711.
Rollwagen-Bollens, G.C., Landry, M.R., 2000. Biological response to iron fertilization in the eastern equatorial Pacific (IronEx II). II. Mesozooplankton abundance, biomass, depth distribution and grazing. Marine Ecology Progress Series 201, 43–56.
Rue, E.L., Bruland, K.W., 1995. Complexation of iron(III) by natural organic ligands in the Central North Pacific as determined by a new competitive ligand equilibration/adsorptive cathodic stripping voltammetric method. Marine Chemistry 50, 117–138.
Schlitzer, R., 2006. Ocean Data View. 〈http://odv.awi.de〉.
Sherr, E.B., Sherr, B.F., 1993. Preservation and storage of samples for enumeration of heterotrophic protists. In: Kemp, P.K. (Ed.), Handbook of methods in aquatic microbial ecology. CRC Press, Boca Raton, FL, pp. 207–212.
Stoecker, D.K., 1999. Mixotrophy among dinoflagellates. Journal of Eukaryotic Microbiology 46, 397–401.
Strutton, P.G., Ryan, J.P., Chavez, F.P., 2001. Enhanced chlorophyll associated with tropical instability waves in the equatorial Pacific. Geophysical Research Letters 28, 2005–2008.
Sunda, W.G., Huntsman, S.A., 1995. Iron uptake and growth limitation in oceanic and coastal phytoplankton. Marine Chemistry 50, 189–206.
Takahashi, T., Sutherland, S.C., Sweeney, C., Poisson, A., Metzl, N., Tilbrook, B., Bates, N., Wanninkhof, R., Feely, R.A., Sabine, C., Olafsson, J., Nojiri, Y., 2002. Global sea-air CO_2 flux based on climatological surface ocean pCO_2 and seasonal biological and temperature effects. Deep-Sea Research II 49, 1601–1622.
Tangen, K., Björnland, T., 1981. Observations on pigments and morphology of *Gyrodinium aureolum* Hulburt, a marine dinoflagellate containing 19'-hexanolyoxyfucoxanthin as the main carotenoid. Journal of Plankton Research 3, 389–401.
Taylor, A.G., Landry, M.R., Selph, K.E., Yang, E.J., 2011. Biomass, size structure and depth distributions of the microbial community in the eastern equatorial Pacific. Deep-Sea Research II 58 (3–4), 342–357.
Twining, B.S., Fisher, N.S., 2004. Trophic transfer of trace metals from protozoa to mesozooplankton. Limnology and Oceanography 49 (1), 28–39.
van den Berg, C.M.G., 1995. Evidence for organic complexation of iron in seawater. Marine Chemistry 50, 139–157.
Vaulot, D., Birrien, J.-L., Marie, D., Casotti, R., Veldhuis, J.W., Kraay, G.W., Chrétiennot-Dinet, M.-J., 1994. Morphology, ploidy, pigment composition and genome size of cultured strains of *Phaeocystis* (Prymnesiophyceae). Journal of Phycology 30, 1022–1035.
Vaulot, D., Marie, D., Olson, R.J., Chisholm, S.W., 1995. Growth of *Prochlorococcus*, a photosynthetic prokaryote, in the equatorial Pacific Ocean. Science 268, 1480–1482.
Verity, P.G., Stoecker, D.K., Sieracki, M.E., Nelson, J.R., 1996. Microzooplankton grazing of primary production at 140°W in the equatorial Pacific. Deep-Sea Research II 43, 1227–1255.
Vesk, M., Jeffrey, S.W., 1987. Ultrastructure and pigments of two strains of the picoplanktonic alga *Pelagococcus subviridis* (Chrysophyceae). Journal of Phycology 23 (2), 322–336.
Wells, M.L., Price, N.M., Bruland, K.W., 1995. Iron chemistry in seawater and its relationship to phytoplankton: a workshop report. Marine Chemistry 48, 157–182.
Wilhelm, S.W., Maxwell, D.P., Trick, C.G., 1996. Growth, iron requirements, and siderophore production in iron-limited *Synechococcus* PCC 7002. Limnology and Oceanography 41, 89–97.
Witter, A.E., Luther III, G.W., 1998. Variation in Fe-organic complexation with depth in the Northwestern Atlantic Ocean as determined using a kinetic approach. Marine Chemistry 62, 241–258.
Wright, S.W., Jeffrey, S.W., 1987. Fucoxanthin pigment markers of marine phytoplankton analyzed by HPLC and HPTLC. Marine Ecology Progress Series 38, 259–266.
Wu, J., Boyle, E., Sunda, W., Wen, L., 2001. Soluble and colloidal iron in the oligotrophic north Atlantic and North Pacific. Science 293, 847–849.
Yoon, H.S., Hackett, J.D., Bhattacharya, D., 2002. A single origin of the peridinin- and fucoxanthin-containing plastids in dinoflagellates through tertiary endosymbiosis. Proceedings of the National Academy of Sciences, USA 99, 11724–11729.
Zar, J.H., 1984. Biostatistical Analysis. Prentice-Hall, Inc., Englewood Cliffs, NJ.